Net Zero

CoSci Press

Review

Carbon Materials for Engineering Active Metal Structures and Reaction Microenvironments in Thermal Catalysis: A Review

Qingsong Luo [1], Yongxiang Chen [2,3], Zengyi Ma [2,3], Haiyu Wei [2], Angjian Wu [2,4], Lei Wang [2,4], Lujie Liu [2,4,*]

1 Key Lab of Biomass Chemical Engineering of Ministry of Education, College of Chemical and Biological Engineering, Zhejiang University, Hangzhou 310027, China

2 State Key Laboratory of Clean Energy Utilization, Zhejiang University, Hangzhou 310027, China

3 Ningbo Global Innovation Center, Zhejiang University, Ningbo 315100, China

4 Inner Mongolia Daqingshan Laboratory, Hohhot, Inner Mongolia 017000, China

Article History:

Received: 1 January 2026

Revised: 11 April 2026

Accepted: 24 April 2026

Published: 30 April 2026

Abstract: Carbon-based materials have demonstrated remarkable potential in heterogeneous catalysis for chemical synthesis, energy conversion, and environmental remediation, owing to their tunable structural properties. In this review, we summarize recent progress in carbon materials optimizing catalytic performance mainly from three aspects: (i) modulation of the geometric and electronic structures of active metal sites through tuning metal-support interactions; (ii) regulation of molecular sorption behaviors during catalysis; and (iii) the synergistic interplay between these two factors, which enables cooperative enhancement of catalytic performance. The wettability of carbon materials can be precisely modulated to facilitate mass transport of reactants and/or products on the catalyst surface, thereby enhancing catalytic performance. In addition, the abundant defect sites and well-developed pore structures of carbon materials can precisely regulate the spatial distribution of metal species and significantly improve their sintering resistance. These insights are expected to offer valuable design principles for the development of highly efficient carbon-based materials for thermocatalytic applications.

Keywords: carbon materials; thermocatalysis; active metal; microenvironment; synergistic regulation

1. Introduction

Carbon materials have exhibited distinct advantages over conventional inorganic supports in heterogeneous catalytic reactions [1,2]. From a sustainability perspective aligned with net-zero emission goals, carbon supports can be derived from abundant and renewable resources (e.g., biomass, waste plastics, and CO_2-derived carbon) [3–5], and their synthesis and processing often require lower energy input compared with high-temperature calcination of inorganic oxides, contributing to reduced carbon footprint and energy consumption [6,7]. On the one hand, carbon materials generally possess high surface areas and tunable pore structures, which enables high dispersion of active metal species and suppress their sintering [8,9]. On the other hand, the excellent electrical conductivity and tunable surface chemistry allow carbon supports to act beyond inert supports by participating in electron transport and interfacial regulation during catalysis [10,11].

The regulation of metal-support interaction (MSI) on conventional reducible metal oxide supports, such as TiO_2 [12–14], CeO_2 [15,16], and Fe_2O_3 [17,18], has been widely discussed. Typical strong metal-support interaction (SMSI) is commonly induced by high-temperature reduction with H_2, which leads to an overlayer of metal oxide on the metal nanoparticle (NP) surface. As a result, the electronic structure of metal NPs is changed to tune the product selectivity, and the

* Corresponding author(s): Lujie Liu, State Key Laboratory of Clean Energy Utilization, Zhejiang University, Hangzhou 310027, China, lujieliu@zju.edu.cn

catalyst stability can be enhanced [19,20]. When using carbon materials as supports, the interaction between metal and support is relatively weak [21,22]. Various strategies have been applied to enhance the MSI in carbon materials, for example, formation of metal-carbon interfaces [23,24] and construction of anchoring sites by heteroatom (e.g., N and S) doping [11,25,26]. In addition, small amounts of carbon materials can serve as promoters, significantly improving catalytic performance in activity [27,28] and/or stability [29].

Previous studies on carbon-supported catalysts have largely focused on improving catalytic performance through structural regulation of active metals, such as tuning metal dispersion, particle size, and metal-support interactions [30,31]. However, recent studies have revealed that carbon materials can also play a critical role in regulating the local microenvironment around active metal sites, for example by modifying surface wettability, adsorption-desorption behavior, and interfacial polarity [32,33]. Such microenvironment modulation provides an alternative pathway to optimize catalytic activity, selectivity, and stability without necessarily altering the intrinsic structure of active metals. More importantly, synergistic regulation of active metal structures and their local microenvironment enables superior performance by coupling key steps in the catalytic process [34,35]. Therefore, summarizing recent advances from the perspectives of active metal structure regulation, microenvironment modulation, and their synergistic interplay can provide a more comprehensive understanding of how carbon materials influence catalytic processes and guide the rational design of carbon-based catalysts.

2. Development of Carbon-Based Materials in Thermocatalysis

As one of the earliest carbon materials employed in heterogeneous catalysis, activated carbon possesses a high surface area, well-developed pore structures, and good thermal stability, and is therefore widely used as a catalyst support for dispersing metal NPs and adsorbing reactant molecules [36]. In addition to its structural features, oxygen-containing functional groups (e.g., hydroxyl, carbonyl, and carboxyl groups) can be introduced onto the surface of activated carbon through appropriate preparation or post-treatment processes, which influence the anchoring of metal species and interfacial interactions to some extent [37]. However, the relatively simple surface chemistry and limited structural tunability of conventional activated carbon restrict precise control over metal-support interactions and the microenvironment of active sites [38].

With the development of carbon nanostructure engineering, carbon nanotubes (CNTs) were introduced into thermocatalysis research in the 1990s [39]. Owing to their one-dimensional tubular structure, high electrical conductivity, and π-conjugated surface, CNTs are able to effectively stabilize metal NPs and modulate metal-support interactions through electronic coupling effects [40,41]. In addition, the curvature of CNTs induces surface strain and charge redistribution, thereby influencing the electronic structure of supported metal species [42]. Their internal hollow structure and mesoporous networks also provide confined spaces that regulate the adsorption-desorption behavior of reactants and intermediates, consequently affecting reaction kinetics and selectivity [43,44].

Entering the early 21st century, the emergence of two-dimensional graphene and its composite materials further expanded the structural diversity of carbon-based supports. Graphene exhibits an ultrahigh specific surface area, high electron mobility, and tunable surface chemistry through defect engineering and heteroatom doping (e.g., N, B, and S) [45]. These characteristics enable more precise control over metal dispersion, electronic structure, and catalytic interfaces. For example, defect sites and doped heteroatoms can serve as anchoring sites for metal species, stabilizing single atoms or ultrasmall clusters while tuning their electronic states [46]. In addition, composite carbon materials such as nanodiamond@graphene combine the structural robustness of nanodiamonds with the high conductivity of graphene, providing a unique platform for constructing well-defined metal-carbon interfaces and facilitating charge transfer [47].

In recent years, advanced carbon architectures, including hierarchical porous carbons and hollow carbon nanostructures, have attracted considerable attention owing to their ability to precisely regulate pore size distribution and spatial confinement effects [48]. In particular, hollow and porous structures can construct confined microenvironments, which not only stabilize encapsulated metal species but also enrich local reactant concentrations, thereby enabling the synergistic regulation of active metal structures and their surrounding microenvironments [49].

In addition to structural design, the catalytic performance of carbon-based materials is also highly dependent on their synthesis parameters and practical operating conditions [50–52]. Factors such as precursor selection, pyrolysis temperature, heating rate, and post-treatment processes can significantly influence the surface chemistry, defect density, pore structure, as well as the dispersion and electronic structure of active metal species [53,54]. For example, high-temperature treatment can enhance the degree of graphitization and electrical conductivity,

but may also lead to heteroatom loss and metal NPs sintering, thereby weakening metal-support interactions [55,56]. In addition, under realistic reaction conditions (e.g., high temperature, the presence of steam, and complex reactant environments), the structure and surface functionalities of carbon materials can dynamically evolve, which further influences the actual structure of active sites and the reaction pathways [57,58].

Over the past decades, the role of carbon-based materials in thermocatalysis has evolved from inert supports dominated by physical adsorption to functional materials with tunable electronic structures, surface chemistry, and reaction microenvironments. These advances have provided important theoretical guidance and new design strategies for developing highly active and stable carbon-based catalysts.

3. Structural Regulation of Active Metals by Carbon Materials

Metal species on the supported catalysts determine the intrinsic activity and selectivity of the reaction, while supports generally indirectly govern the overall catalytic performance by modulating the state of the active metals [59]. For carbon materials, they can regulate metal species through multiple strategies, including MSI, spatial confinement, and dopant-induced effects. Such regulation exerts a significant impact on the catalytic performance.

3.1. Metal Size Modulation

The delocalized π-electrons of carbon materials can effectively couple with the *d* orbitals of metals, enabling orbital hybridization and charge transfer [60,61]. This redistribution of charge alters the electronic density and Fermi level of the active metals, thereby modulating their adsorption energy toward reactant molecules and influencing the reaction pathway [62]. Furthermore, the atomic arrangement, layered structure, and surface defects of carbon materials can induce the oriented growth and ordered distribution of metal atoms at the interface, thus enabling stepwise control over the metal structure from single atoms (SAs) to clusters and eventually to NPs [62]. This process is often accompanied by changes in the electronic structure of the metal species, which affects the adsorption configuration of chemical molecules during the reaction and regulates the reaction pathway [62–64] (Figure 1A). In the formic acid dehydrogenation reaction, when the Pd NP size on the carbon support decreases from 4.5 to 2.1 nm, the catalytic activity increases significantly by approximately 3.6 times, reaching a turnover frequency (TOF) of 835 h^{-1}. With the reduction in metal particle size, the Pd dispersion increases, accompanied by a larger proportion of positively charged Pd species. The enhanced interaction between these positively charged Pd species and the negatively charged formate ions (the key reaction intermediates) significantly promotes the reaction [65].

Compared with conventional supported metal catalysts, carbon-supported single-atom catalysts (SACs) exhibit enhanced MSI due to the electronic interaction between the isolated metal atoms and the carbon support [66]. Such interaction precisely regulates the adsorption-activation behavior of reactant molecules and the associated reaction energy barriers, thereby enabling outstanding catalytic performance in typical thermal catalytic reactions such as oxidation, hydrocarbon reforming, hydrogenation/dehydrogenation, and ammonia decomposition [66–70]. Notably, the intrinsically high surface free energy of SACs leads to thermodynamic instability, causing metal species to readily undergo aggregation and sintering during reactions to reduce the system free energy (Figure 1B) [71]. In contrast, metal cluster catalysts, with sizes between SAs and NPs, exhibit superior overall catalytic performance in complex reaction systems [4,52]. For example, Liu et al. [72] prepared Ni-based SAs, clusters, and NPs catalysts by controlling the Ni loading on nanodiamond@graphene for acetylene semi-hydrogenation. The desorption of ethylene is more favorable on the Ni cluster catalyst, thereby suppressing the over-hydrogenation of ethylene to ethane. As a result, full acetylene conversion with 85% ethylene selectivity at 190 °C was achieved.

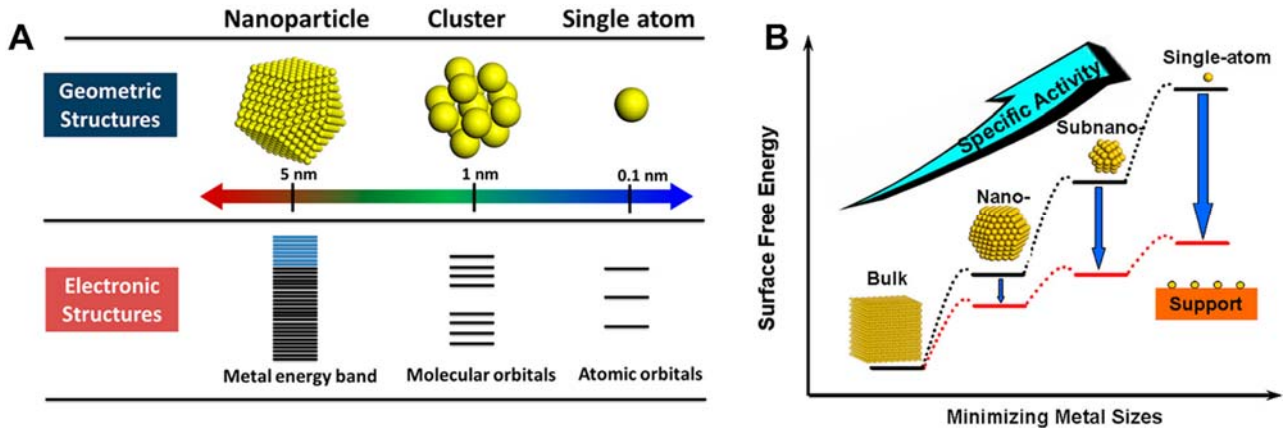

Figure 1. Size effects on electronic structure and surface energy. (A) Geometric and electronic structures across single atoms, clusters, and nanoparticles [63]. (B) Schematic showing how surface free energy and per-metal-atom activity depend on particle size, as well as the stabilizing effect of the support on single atoms [71].

3.2. Spatial Confinement of Metal Species in Carbon Materials

The encapsulation of metals within carbon materials can induce a pronounced confinement effect [43]. The electronic transfer and chemical bonding interactions between carbon support and the encapsulated metal species can shift the *d*-band center of the metals, thereby modulating the adsorption and activation of reactant molecules [73]. Meanwhile, the nanoscale pores within the carbon matrix provide confined spaces for the active metals, effectively suppressing their migration and aggregation, thereby enhancing catalyst stability. In addition, the well-defined and tunable nanoporous channels of carbon materials can regulate molecular diffusion and adsorption configuration, which would accelerate reaction kinetics and further boost activity.

Carbon nanotubes, featuring a unique one-dimensional hollow structure with tunable inner diameters, provides an ideal platform for investigating confinement effects [44] . Bao et al. performed a series of insightful studies on CNTs-based confined catalysis. CNTs are formed by the curvature of graphene layers, which causes the π-electron density to shift from the concave inner surface to the convex outer surface, resulting in a potential difference across the CNT walls [43]. This potential difference can influence the electronic properties of active metal species in contact with either surface. For example, the reduction temperature of Fe_2O_3 NPs encapsulated within the nanotube channels is approximately 200 °C lower than that on the outer surface of CNTs (Figure 2A). Moreover, as the inner diameter of the CNTs decreases from 8-12 nm to 2-5 nm, the reduction temperature of the encapsulated Fe_2O_3 further decreases [74]. The electronic interaction between the CNTs and the metals downshifts the *d*-band states of the metal clusters confined within the nanotubes, and the adsorption strength of molecules (such as CO, N_2, and O_2) on the encapsulated metal clusters is weakened (Figure 2B). Consequently, the oxygen species can be more readily removed by a reducing agent, making the confined metal oxide easier to reduce [75]. Fischer-Tropsch synthesis (FTS) is an important reaction for converting syngas (a mixture of CO and H_2) into long-chain hydrocarbons, which is highly dependent on the oxidation state of Fe species [76]. Owning to the confinement effect, Fe species encapsulated within the inner channels of CNTs are prone to be reduced and transformed into active iron carbides under reaction conditions (Figure 2C,D). Such catalyst (Fe_2O_3-*in*-CNT) shows nearly twice the yield of C_5^+ hydrocarbons compared to the Fe_2O_3-*out*-CNT catalyst with Fe species dispersion on the outer surface of CNTs under the same conditions (Figure 2E) [77].

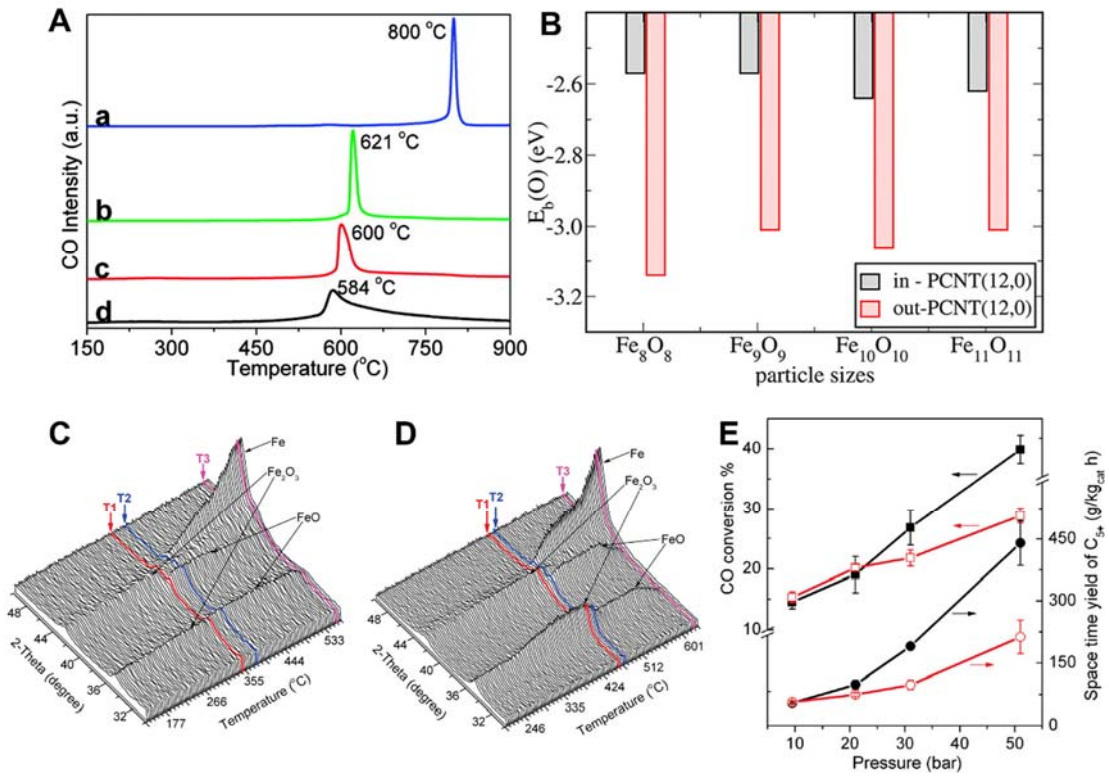

Figure 2. The confinement effect of CNTs on metal species. (A) CO evolution during TPR of different Fe_2O_3/CNT samples. (a) Fe_2O_3-*out*-CNT(4); (b) Fe_2O_3-*in*-CNT(8); (c) Fe_2O_3-*in*-CNT(4); (d) Fe_2O_3-*in*-CNT(2) [74]. Oxygen binding energies E_b(O) of Fe_nO_n (n= 8-11) clusters confined within PCNT(12, 0) (in-PCNT) compared with those located on the outer wall (out-PCNT) [75]. *In situ* XRD monitoring of the temperature-programmed reduction in 10% H_2/Ar for (C) Fe_2O_3-*in*-CNT and (D) Fe_2O_3-*out*-CNT [77]. T1: FeO emerges; T2: Fe appears; T3: FeO disappears. (E) FTS activity of Fe-*in*-CNT and Fe-*out*-CNT. Filled symbols represented Fe-*in*-CNT and open ones represented Fe-*out*-CNT [77].

On the other hand, the confined environment further hinders the migration of metal species [78]. The carbon layer can be formed on the surface of Ni NPs (Ni@C) through high-temperature carbonization [79]. The carbon layer formed during high-temperature carbonization encapsulates the Ni NPs, effectively suppressing particle growth and leading to smaller metal particle sizes than those of directly deposited metal catalyst (NiO/C). As a result, Ni@C exhibits negligible Ni NPs sintering and maintains stable catalytic activity during low-temperature liquid-phase hydrogenation of sodium *p*-nitrobenzoyl glutamine for over 550 h. It should be noted that the encapsulation of metal NPs by carbon layers inevitably covers part of the active metal surface, leading to reduced catalytic activity [80]. Recent studies have pointed out that encapsulation of metal NPs within microporous/mesoporous materials would result in a larger exposed surface area, which can provide more accessible active sites for durable catalysis [81,82]. Zong et al. [83] used a novel honeycomb-structured graphene (HSG) with uniformly distributed macropores of ~50-70 nm in diameter to stabilize Fe NPs in the CO_2 hydrogenation to light olefins (Figure 3A). The unique three-dimensional porous architecture of HSG spatially confines the active iron carbide NPs formed under reaction conditions, effectively suppressing their high-temperature aggregation and maintaining stable catalytic activity over 120 h (Figure 3B). Fe NPs with tunable particle sizes can be encapsulated in mesoporous carbon using the templating method (Figure 3C), allowing precise control over olefin and paraffin selectivity in FTS [84]. Moreover, the mesoporous carbon matrix effectively suppresses NPs migration during reaction, leading to outstanding catalytic stability. No discernible performance degradation is observed after reaction for 100 h, and particle size growth is negligible (Figure 3D).

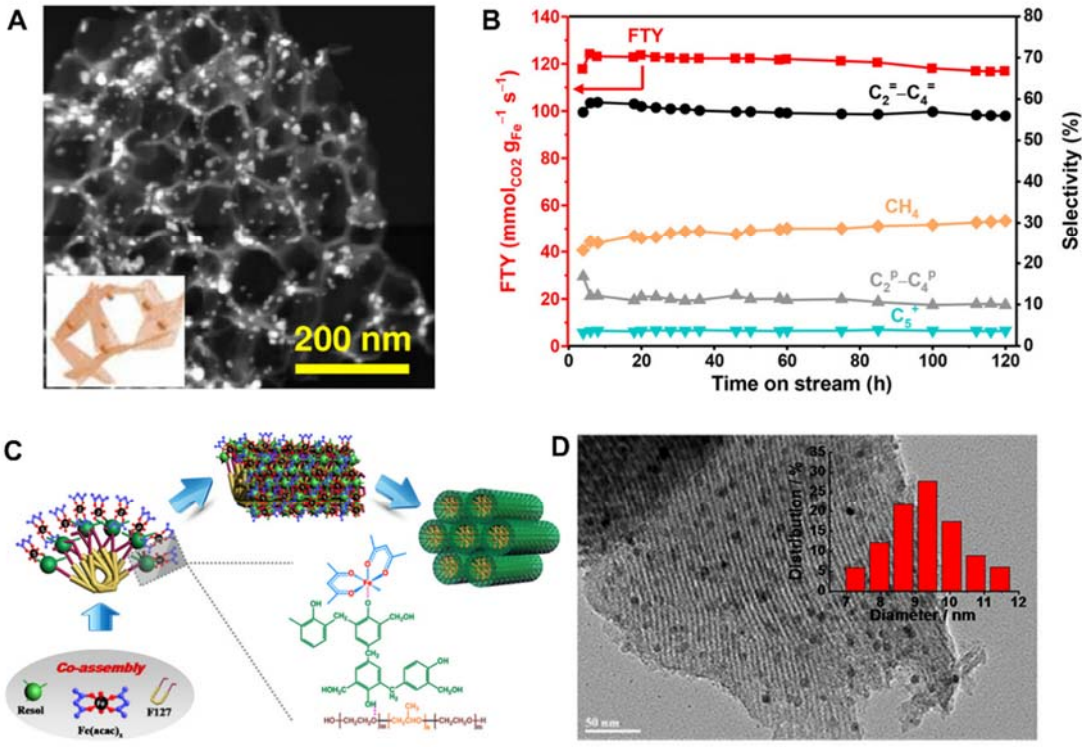

Figure 3. The spatial confinement of carbon materials in stabilizing metal species. (A) TEM image of the FeK1.5/HSG catalyst [83]. (B) Catalytic performance of FeK1.5/HSG in the CO_2 hydrogenation to light olefins over120 h [83]. (C) Illustration of the synthesis of the Fe-based nanoparticles incorporated ordered mesoporous carbon (Fe-C-8) [84]. (D) TEM image and average particle size distributions of used Fe-C-8 catalysts in Fischer-Tropsch synthesis [84].

Bao et al. [85] reported the RhMn NPs encapsulated within CNTs exhibited no noticeable deactivation after syngas-to-ethanol reaction for 112 h. The particle size of those confined inside the nanotube channels was approximately 4-5 nm, whereas the particles located on the outer surface grew to ~8 nm after reaction. In addition, with the similar structure, the Fe NPs size encapsulated within CNTs remained unchanged (4-8 nm) during the FTS reaction for 200 h, whereas the Fe NPs grew to 12-16 nm on the outer-surface of CNTs [77]. These results demonstrated that the confinement structure of CNTs effectively suppresses metal migration and sintering, thereby enhancing the catalyst stability.

3.3. Dopant-Induced Effect

Heteroatoms, such as nitrogen (N) [86,87], phosphorus (P) [88,89], boron (B) [90,91], and sulfur (S) [92,93], possess distinct electronegativities and orbital configurations, and their incorporation into the carbon framework modulates the electronic state of metal species through heteroatom-induced charge redistribution. In the case of an N-doped carbon-supported cobalt catalyst, the hybridization between the Co *3d* orbitals and N *2p* orbitals leads to the formation of Co-N bonds, which enriches the *d*-electron density of Co. As a result, the electrons can transfer from the Co *3d* orbitals to the π* antibonding orbitals of N_2 in the ammonia synthesis, thereby lowering the activation energy for N_2 and promoting the reaction under mild conditions [94]. The B atom, with its relatively low electronegativity, can also stabilize metal species in low or zero oxidation states by modulating the metal-support electronic interactions. This electronic regulation facilitates hydrogen activation and thereby accelerates reaction kinetics, ultimately enhancing the efficiency of the semi-hydrogenation of 1,3-butadiene [95]. Compared with single-element doping, co-doping with two or more heteroatoms can generate multiple coordination environments, such as M-N_xP_y or M-N_xS_y, where M represents metals [96–98]. Compared with the symmetric Co_1-N_4 configuration, heteroatom P incorporation breaks the electronic symmetry and generates an asymmetric coordination environment in the single-atom Co_1/NPC catalyst. This modulation upshifts the Co *d*-band center toward the Fermi level, enhancing antibonding state occupation between Co and adsorbed H_2, thereby facilitating H_2 dissociation and endowing Co_1/NPC with markedly enhanced hydrogenation activity [99].

Sulfur is widely recognized as a poisoning element for heterogeneous catalysts [100]; however, recent studies have revealed that by precisely tuning its coordination environment

with metal species, S can selectively poison specific metal facets, modulate the adsorption configurations and reaction pathways of reactants, and ultimately enhance catalytic activity and selectivity [101]. In the case of carbon materials, S can incorporate into carbon-based supports and generate meta-sulfur (M-S) interfacial sites, which can serve as the dominant active centers for catalytic hydrogenation by synergistically regulating the adsorption and activation of substrates (Figure 4A). The intrinsic catalytic activity of the Ir-S interface (~800 mol mol_{Ir}^{-1} min^{-1}) in quinoline hydrogenation is nearly 53 times higher than that on the metallic Ir surface (~15 mol mol_{Ir}^{-1} min^{-1}, Figure 4B,C). Mechanistic studies revealed that H_2 dissociation occurs on surface Ir atoms, while quinoline activation is promoted at the Ir-S interfacial sites. Moreover, the interfacial Ir-S electronic interaction enriches the electron density of the Ir clusters, which consequently reduces the desorption barrier of 1,2,3,4-tetrahydroquinoline and mitigated catalyst deactivation (Figure 4D). Interestingly, similar interfacial effects were also observed in *p*-chloronitrobenzene hydrogenation over the Pt-S interfaces and benzoic acid hydrogenation over the Ru-S interfaces [102].

The electronic metal-support interaction (EMSI) between metals and S-doped carbon (S-C) endows the S-C-supported catalysts with exceptional sintering resistance. For example, the S-C support stabilizes metal NPs (Pt, Ru, Rh, Os, and Ir) at metal size around 1 nm even after thermal treatment at 700 °C for 10 h [103]. Notably, the S content on the support remains nearly unchanged, indicating that the S-C framework is thermally stable. In contrast, severe sintering occurred for Pt NPs supported on S-free carbon (S-free-C) and N-doped carbon under the same conditions. Density functional theory calculations (Figure 4E) revealed that the adhesion energy between Pt and the S-C support was significantly increased due to Pt species bonding to S. As a result, higher diffusion barrier and/or migration barrier of Pt species effectively suppressed metal agglomeration. In propane dehydrogenation, the electron-rich Pt NPs on the S-C support weakened the interaction between Pt and the π-bonded C=C group of propylene, thereby facilitating product desorption and resulting in outstanding coke resistance of the catalyst (Figure 4F).

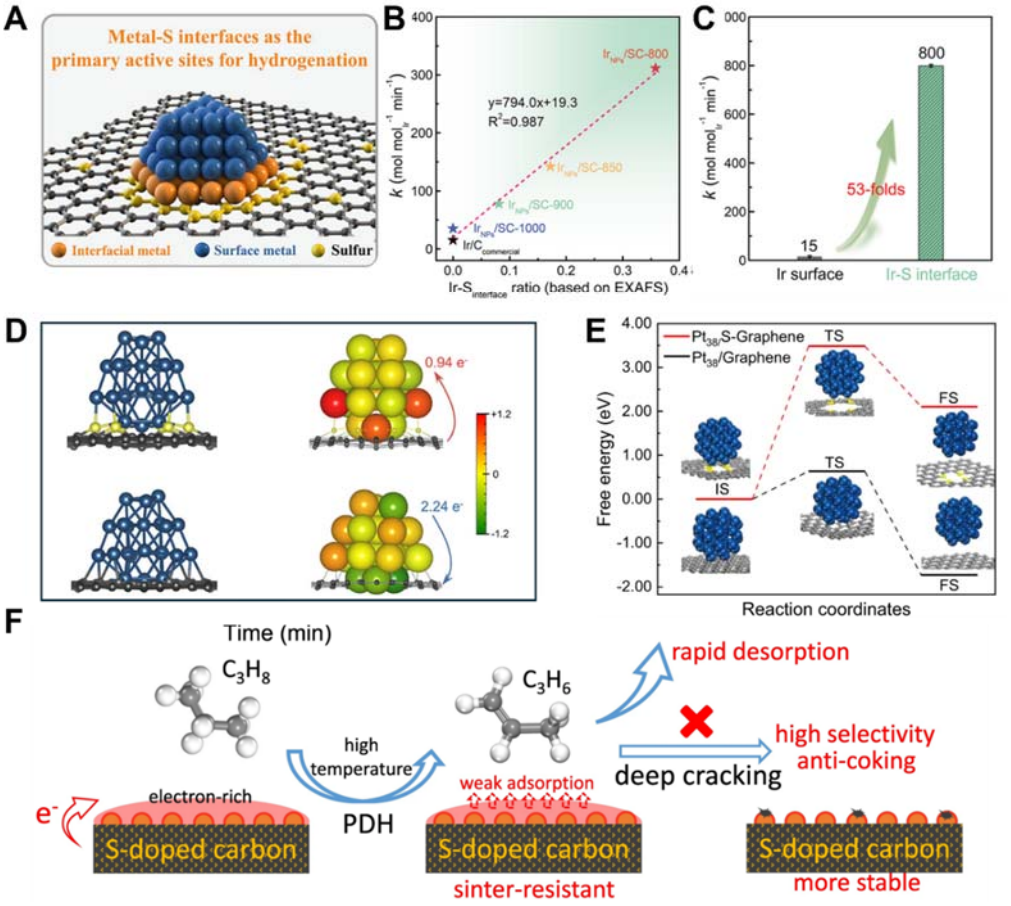

Figure 4. The enhancement of catalytic performance induced by S-doped carbon materials. (A) Schematic diagram of Ir_{NPs}/SC-*x* catalysts [102]. (B) Ir-normalized reaction rates plotted as a function of the Ir-S interface ratio for different samples [102]. (C) The quinoline hydrogenation reaction rates of the Ir-S interface and Ir surface. (D) Schematic models and Bader charges of Ir of Ir_{22}/SC (top) and Ir_{22}/VC (bottom), where Ir, S, and C atoms were depicted in blue, yellow, and gray, respectively [102]. (E) Energy barrier of Pt_{38} cluster of S-Graphene and Graphene [103]. (F) Schematic illustration highlighting the vital role of interfacial electronic interactions between Pt and S-C in enhancing the selectivity and stability of the propane dehydrogenation reaction [103].

When carbon materials are used as promoters, they can also regulate the electronic and geometric structures of metal species, thereby improving catalytic performance. Cu-based catalysts are widely investigated for the hydrogenation of dimethyl oxalate to ethylene glycol. However, their performances are widely constrained by insufficient H_2 activation and the difficulty of stabilizing Cu^+ species, whereas harsher reaction conditions further promote Cu sintering [104]. To address these issues, Xie et al. [28] introduced fullerene (C_{60}) into Cu/SiO_2 catalysts as an electron buffer, stabilizing Cu^+ species via reversible electron transfer and markedly enhancing hydrogen activation. As a result, the catalyst (C_{60}-Cu/SiO_2) exhibited exceptionally high activity, enabling the hydrogenation of dimethyl oxalate to ethylene glycol under ambient-pressure conditions, while maintaining stable performance for 1000 h in kilogram-scale reactions. In a different approach, Xiao et al. [29] loaded chemically inert carbon species around Cu NPs to create weak-interaction regions, which substantially increased the free-energy barrier for surface migration of Cu particles or atomic Cu intermediates, thereby effectively suppressing Cu sintering.

4. Modulation of the Catalyst Microenvironment by Carbon Materials

During catalytic reactions, the catalytic performance is governed not only by the intrinsic structure of active metals but also by their surrounding microenvironment. Carbon materials can precisely regulate the microenvironment around the active metals at nanoscale, thereby influencing key steps such as reactant enrichment, activation, and product desorption.

4.1. Molecular Sieving and Adsorption Effects in Carbon Materials

The well-defined nanoporous architecture in carbon materials can selectively adsorb reactant molecules with specific sizes or configurations. Such preferential adsorption and confinement effects alter the local concentration and orientation of molecules around active metals, thereby optimizing the catalytic performance by altering the reaction kinetics [44,105]. The strong adsorption of N-heteroarenes on metal surfaces often leads to metal poisoning and leaching [106–108]. By encapsulating the metal NPs within the porous carbon with a pore size of ~0.53 nm, the pores allow H_2 to access and dissociate on internal Co sites while excluding N-heteroarenes from direct contact with the Co surface. The generated active hydrogen species then migrate to the carbon surface via hydrogen spillover, where N-heteroarenes are efficiently hydrogenated. This pore-size sieving effect of carbon suppresses metal poisoning and enhances both catalytic activity and stability [109]. And the pore-size sieving effect can also enable effective regulation of reaction pathways in complex catalytic systems, thereby improving the product selectivity. In the synthesis of the imine *N*-(9-phenanthrenylmethylene) aniline, nitrobenzene preferentially diffuses into the interior of PdCu@hollow carbon spheres (PdCu@HCS) and is rapidly reduced to aniline, which subsequently condenses with phenanthrene-9-carboxaldehyde outside the carbon shell to form the target imine (Figure 5A). The imine product cannot diffuse through the carbon shell and is therefore protected from over-hydrogenation, whereas PdCu NPs exposed on the external surface of PdCu/HCS further hydrogenate the imine to the corresponding amine, resulting in reduced catalytic selectivity (Figure 5B) [110].

The pore-size effect of carbon materials is predominantly based on the difference in molecular size and geometry; however, it becomes less effective for distinguishing molecules with comparable size and geometry. In such cases, chemical selectivity derived from carbon-molecule interactions, including van der Waals forces and π-π interactions, becomes critically important [111]. Bao et al. [112] employed first-principles calculations combined with Monte Carlo simulations to investigate the interactions and adsorption distributions of CO and H_2 on CNTs (a curved pyrene $C_{16}H_{10}$ cluster model) during syngas conversion (Figure 5C). The binding energies of both CO and H_2 on the inner surface of CNTs were found to be higher than those on the outer surface, indicating that these molecules are more readily adsorbed within the nanotube channels. Because of its larger dipole moment, CO forms stronger polarization interactions with the CNT wall, while the nonpolar H_2 molecules interact only weakly through van der Waals forces. As a result, CO interacts more strongly with the inner surface of CNTs, leading to its selective enrichment inside the nanotubes, which is beneficial for enhancing the reaction rates and tuning product selectivity (Figure 5D). Xiao et al. [113] demonstrated that π-π interactions between the phenyl ring framework of poly(divinylbenzene) (PDVB) and the aniline product facilitate its rapid desorption from the Pd NP surface, thereby preventing catalyst poisoning and enabling highly efficient solvent-free hydrogenation of nitrobenzene to aniline (Figure 5E,F).

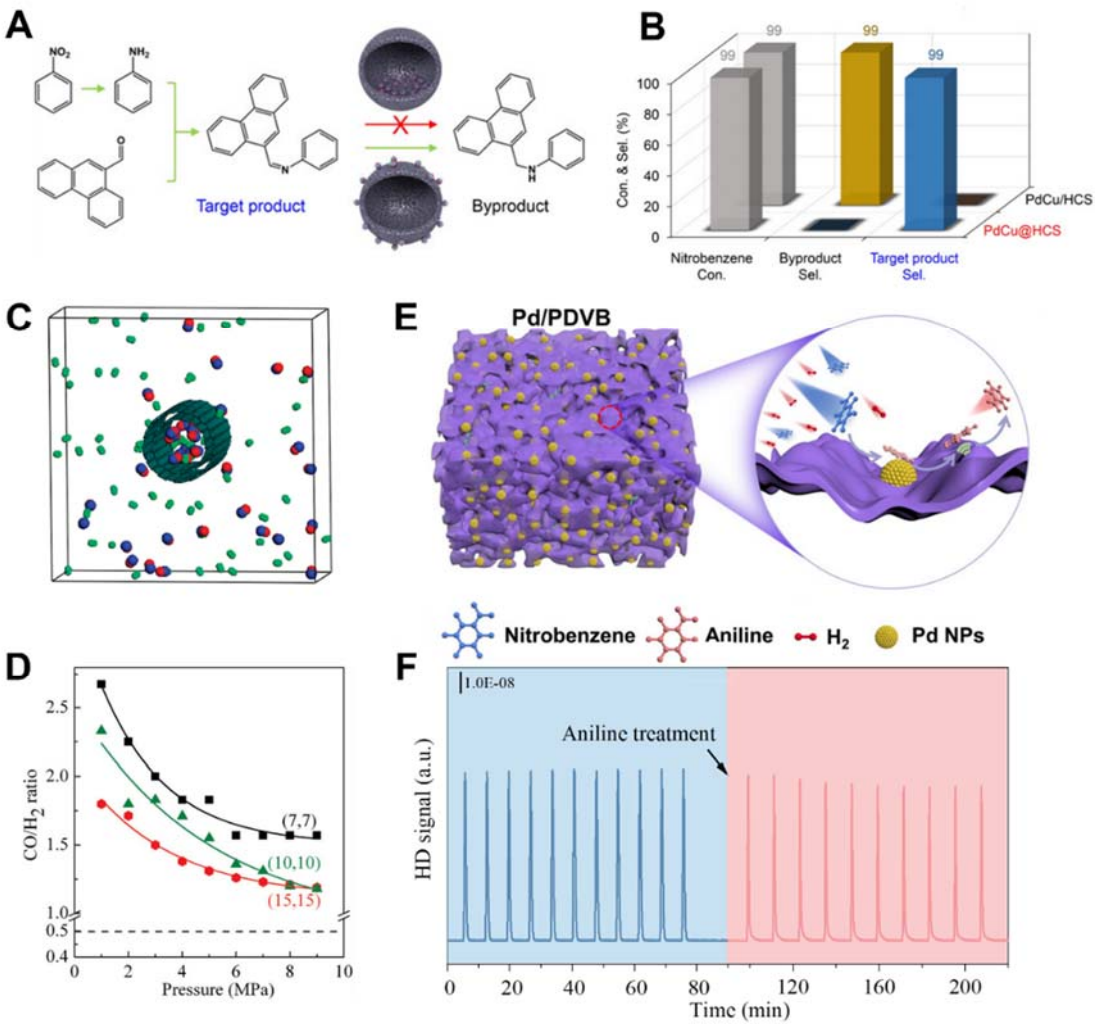

Figure 5. Reactant enrichment and facilitated product desorption induced by carbon materials. (A) Schematic illustration of the cascade reductive coupling reaction between nitroarenes and carbonyl compounds [110]. (B) Catalytic performance of the cascade reaction over PdCu@HCS and PdCu/HCS. (C) Simulation model of a (10, 10)-(13, 13) DWNT placed in a box of (66.5 × 66.5 × 24.4 Å^3). Blue and red spheres represented CO, while light green spheres denoted H_2 [112]. (D) Variation of the CO/H_2 ratio inside CNTs with different diameters as a function of pressure, where the dashed line denoted the CO/H_2 ratio (0.5) in the gas phase [112]. (E) Schematic illustration of solvent-free nitrobenzene hydrogenation over Pd/PDVB [113]. (F) H-D exchange studies on Pd/PDVB in the presence and absence of aniline, respectively [113].

4.2. Adjustable Hydrophilicity of Carbon Materials

Introducing oxygen-containing functional groups (-OH, -COOH, -C=O, etc.) onto the catalyst surface can enhance interactions with oxygenated reactants (e.g., alcohols, phenols, and carboxylic acids) through hydrogen bonding and polar interactions, which promotes reactant adsorption and favors subsequent catalytic conversion [114,115]. Therefore, moderately enhancing the hydrophilicity of catalysts has been proven to be an effective strategy for improving their performance in biomass conversion processes. Surface oxygen-containing groups can also modulate the reaction pathway and thereby alter the reaction selectivity. For example, oxygen functional groups on CNTs were found to inhibit the hydrogenation pathway by blocking the adsorption and/or migration of guaiacol on active sites, while simultaneously promoting the formation of dimethoxymethane [116]. In addition, oxygen-containing functional groups on the carbon support also exhibit strong Brønsted acidity that facilitates the dehydration process and cooperated with the Lewis acidic metal centers to synergistically activate the reactant molecules [117] .

Recent studies have also revealed that hydrophobic catalyst surfaces can regulate the interfacial microenvironment in gas-liquid-solid reactions, thereby significantly influencing reactant mass transfer [33,118]. A hydrophobic surface can effectively prevent active metals from being covered by water or polar molecules and subsequently oxidized or deactivated at

high temperature [119,120]. In addition, hydrophobicity facilitates the enrichment and diffusion of gaseous reactants at the interface, thereby enhancing the efficiency of gas-liquid interfacial reactions. By introducing the graphdiyne (GDY) nanospheres into the mesopores of $Pd/mSiO_2$, the originally hydrophilic channels are converted into hydrophobic ones [121] (Figure 6A). The resulting $GDY@Pd/mSiO_2$ with superhydrophobic surface exhibits remarkable aerophilicity in water, enabling gas enrichment within 60 ms, whereas the hydrophilic $Pd/mSiO_2$ fails to capture the gas even after 10 s (Figure 6B). During the reaction, the hydrophobic pores of $GDY@Pd/mSiO_2$ allow H_2 to fill and be stored inside the mesopores at a concentration much higher than that in the aqueous phase. In contrast, the unmodified $Pd/mSiO_2$ pores are filled with water, and H_2 is supplied only in its dissolved form, resulting in an extremely low H_2 concentration near Pd NPs (Figure 6C). Consequently, $GDY@Pd/mSiO_2$ enables efficient hydrogenation of benzaldehyde in water under ambient H_2 pressure, achieving a 4.3-fold higher catalytic activity than the unmodified $Pd/mSiO_2$ catalyst (Figure 6D). In contrast to employing GDY nanospheres as hydrophobic additives, directly employing the hydrophobic carbon material PDVB as the support has also been demonstrated to effectively enrich reactant molecules [32]. The strong interaction between pyridine and PDVB promotes catalyst dispersion in water (Figure 6E), which is beneficial for enhancing catalytic activity. More importantly, the hydrophobic microenvironment of PDVB enhances hydrogen mass transfer in the aqueous phase and local hydrogen availability at Ru NPs, enabling efficient pyridine hydrogenation under ambient hydrogen pressure. (Figure 6F,G). These features result in Ru/PDVB with exceptionally high catalytic activity, far surpassing that of previously reported catalysts (Figure 6H). In addition, this interaction weakens the direct contact between Ru NPs and pyridine, thereby endowing the catalyst with improved stability (Figure 6I). These works highlight that constructing a hydrophobic interfacial microenvironment by carbon materials can significantly enhance local gas availability and facilitate efficient gas-liquid-solid mass transfer, thereby providing an effective approach for achieving high-performance three-phase reactions under mild conditions.

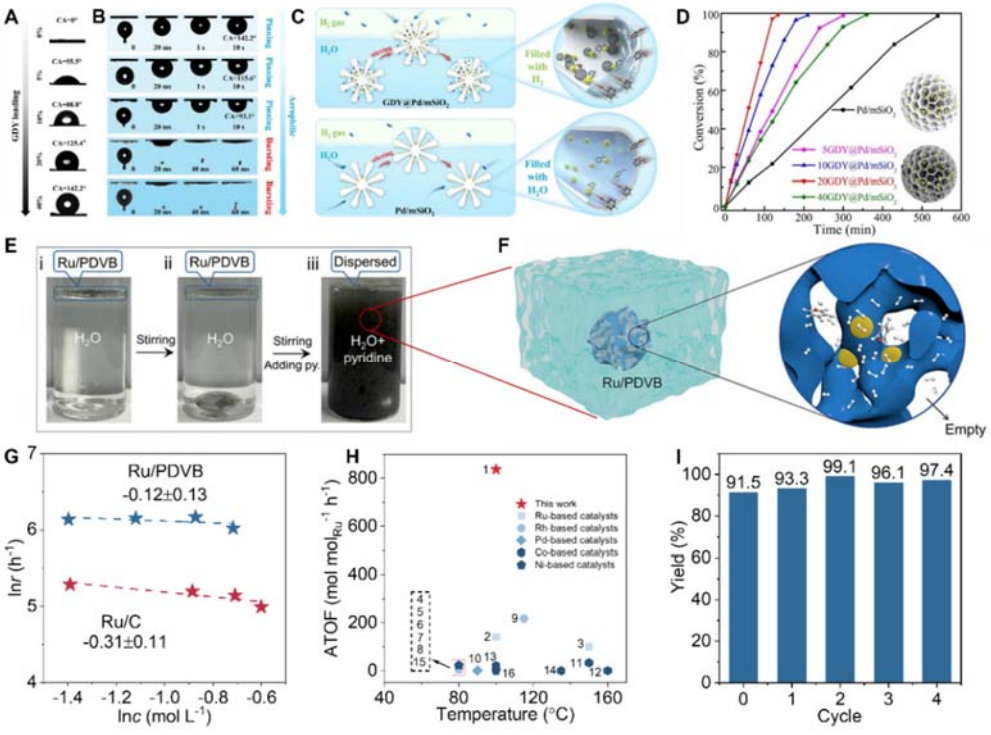

Figure 6. Carbon materials function as the hydrophobic additive and support to facilitate gas enrichment in three-phase catalytic reactions. (A) Water contact angles and (B) H_2 gas-bubble contact angles under water of $Pd/mSiO_2$ and $GDY@Pd/mSiO_2$ [121]. (C) Schematic illustrations of the reactions taking place on hydrophobic $20GDY@Pd/mSiO_2$ and hydrophilic $Pd/mSiO_2$ catalysts. White flower-like structures, yellow spheres, and black spheres correspond to $mSiO_2$, Pd NPs, and GDY nanospheres, respectively [121]. (D) The catalytic performance of various catalysts for benzaldehyde conversion [121]. (E) Photographs of the dispersion state of the Ru/PDVB in water and pyridine aqueous solution [32]. (F) Schemes illustrating the gas enrichment of Ru/PDVB during pyridine hydrogenation in water [32]. (G) The hydrogen reaction order over Ru/PDVB and Ru/C catalysts, respectively [32]. (H) Average turnover frequency and (I) stability test of Ru/PDVB in the pyridine hydrogenation in water [32].

In the FTS process, the production of water had detrimental effects on catalytic performance [122–124]. Water molecules compete with CO and H_2 for adsorption on active metals, blocking reactant diffusion and thereby reducing catalytic activity. In addition, water induces side reactions, for example, the water-gas shift reaction, leading to the low selectivity of olefins. More importantly, the active species (e.g., Co^0 and Fe_5C_2) can be oxidized under elevated water partial pressure at high rection temperature, which would cause metal sintering and catalyst deactivation. Therefore, suppressing the accumulation of water on the surface of active metals is of great significance. Through the encapsulation of TiO_2 with a hydrophobic carbon layer, a robust $Ru/TiO_2@C_{DA}$ catalyst with exceptional sintering resistance was constructed [125]. Mechanistic studies revealed that the carbon encapsulation reduced surface hydroxyl groups, effectively suppressing the oxidation-reduction pathway and preventing metal aggregation. Moreover, the absence of Ru-TiO_2 interfacial sites in $Ru/TiO_2@C_{DA}$ promotes *CO adsorption while suppressing *H adsorption, facilitating carbon-chain growth and ultimately achieving a high C_{15}^+(soft paraffin) selectivity of 57.3%. Silane modification and surface functionalization can also enhance the hydrophobicity of catalysts to improve their performance in FTS process [126,127]. However, these approaches inevitably lead to partial coverage of the active metals and reduced the intrinsic activity of the catalyst.

Simple physical mixing of the catalyst with hydrophobic carbon materials provides an effective and straightforward strategy to promptly remove *in situ*-generated water without altering the catalyst structure. Xiao et al. [128] proposed a simple and general strategy by physically mixing PDVB with the CoMnC catalyst to construct a locally hydrophobic environment that facilitates water desorption, thereby promoting CO hydrogenation (Figure 7A). The pristine CoMnC catalyst exhibited a CO conversion of 32.2% and a C_2-C_4 olefin selectivity of 60.8%, whereas the mixed CoMnC/PDVB catalyst achieved a markedly higher CO conversion of 63.5% and an olefin selectivity of 71.4% under identical conditions (Figure 7B). Furthermore, the CoMnC/PDVB catalyst showed excellent durability with stable CO conversion of 62.8% and constant light olefins at 70.0% after 120 h of continuous reaction (Figure 7C). CO pulse experiments (Figure 7D) showed that both CoMnC and CoMnC/PDVB catalysts adsorbed CO effectively in the absence of water. When the water was introduced, CO adsorption on CoMnC catalyst was significantly suppressed due to the competitive adsorption of water, whereas CO adsorption on CoMnC/PDVB remained unchanged, demonstrating that PDVB suppressed the water adsorption on the surface of catalyst. Theoretical simulations (Figure 7E–G) further revealed that PDVB promoted rapid water desorption, exposed more active sites for continuous CO conversion and consequently improved the efficiency of the FTS reaction. A similar phenomenon was also observed in CO_2 hydrogenation to methanol [129], further confirming that the physical regulation of catalysts with suitable carbon materials holds great promise for guiding the rational design of efficient catalysts in the future.

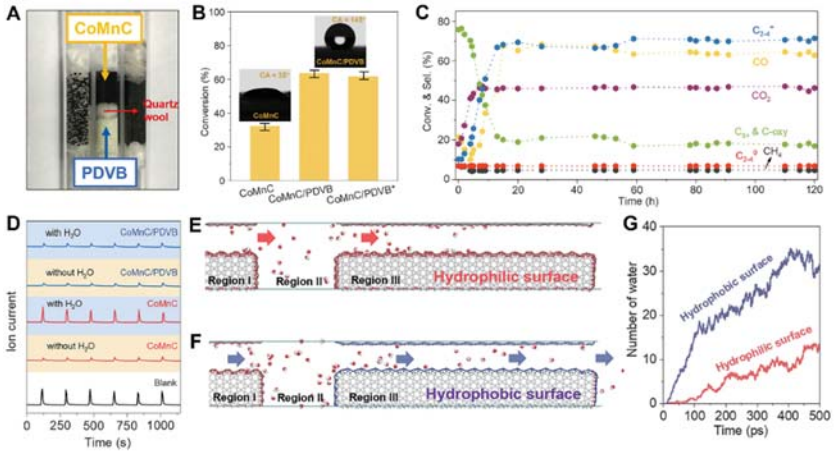

Figure 7. Promotion of water desorption by the physical mixing of carbon materials with catalysts [128]. (A) Photographs of the catalyst beds prepared by different mixing methods. (B) Catalytic performance data over different catalysts for FTS conversion. (C) Stability evaluation of the CoMnC/PDVB catalyst during FTS conversion. (D) Transient response profiles recorded during 10% CO/He pulse experiments under a He flow at 250 °C over CoMnC and CoMnC/PDVB catalysts. (E and F) Schematic models illustrating water removal through different regions; region I was hydrophilic, while region III exhibited both hydrophilic and hydrophobic characteristics. (G) Number of water molecules escaping from region III over time, starting from an initial configuration containing 100 water molecules adsorbed on region I.

5. Synergistic Regulation of Metal Structure and Microenvironment

Although carbon materials have been widely demonstrated to enhance catalytic performance via the independent tuning of active metal structures and their surrounding microenvironments, these two factors are inherently interconnected in practical catalytic systems and collectively regulate reaction pathways and kinetic behaviors. The encapsulation of metals within porous carbon materials represents a typical example. On the one hand, meta-carbon interfacial interactions can modulate the dispersion state and electronic structure of metal species, while the confinement effect suppresses metal aggregation, thereby improving catalyst stability. On the other hand, the porous carbon framework regulates the mass transport of reactants and/or products through its tunable pore structure and surface properties.

Wang et al. [130] constructed an efficient hydrogenation catalyst (RGO@AC/Pd) by encapsulating Pd within double-shelled hollow carbon nanospheres (RGO@AC). The confined interface between the carbon framework and metal species enabled atomically dispersed Pd and suppressed aggregation. Meanwhile, the unique hollow and nanoporous architecture facilitated reactants diffusion and mass transport, leading to local enrichment of substrates around the active sites. The synergy between structural regulation and microenvironment modulation endowed the catalyst with outstanding activity and stability in the reduction of 4-nitrophenol and Suzuki coupling reactions. Compared with single-atom catalysts, alloy catalysts offered more diverse active site configurations and stronger synergistic regulation in heterogeneous thermal catalysis [131,132]. However, structural evolution during reaction, such as metal aggregation and phase segregation under harsh conditions, often limited their practical application [132]. Porous carbon materials, owing to their high thermal stability and unique confinement effect, were widely regarded as ideal supports for stabilizing alloy structures. Meanwhile, the confined microenvironment they provided regulated the adsorption-desorption behavior of reactants and intermediates, thereby enabling additional control over reaction pathways [133,134]. Dong et al. [135] reported that encapsulating PdCu alloys within a carbon layer significantly enhanced the performance of acetylene semi-hydrogenation. The confinement effect of the carbon layer suppressed the growth of carbon chains into longer oligomers or polymers, thereby reducing the formation of green oil and improving ethylene selectivity. Meanwhile, the confinement of metal NPs effectively inhibited particle sintering, leading to enhanced structural stability of the catalyst. Owing to the synergy between structural regulation and microenvironment modulation, the catalyst maintained stable operation for over 150 h with an acetylene conversion of ~98% and an ethylene selectivity of ~90%, highlighting the advantages of such synergistic effects in selective hydrogenation reactions. Interestingly, in addition to stabilizing the alloy structure, the unique core-shell structure further enhanced the performance of the reverse water-gas shift hydrogenation reaction by promoting spillover processes [136].

With the accumulation of extensive experimental evidence, it became increasingly clear that the spatial confinement effect in porous carbon materials (particularly HCSs) did not originate from a single factor, but rather represented a synergistic outcome. Lu et al. [137] systematically investigated HCSs with tunable curvature and carbon shell thickness, synthesized via a hard-templating method, in the hydrogenation of levulinic acid to γ-valerolactone. Their study elucidated the coupled roles of metal-support electronic interactions, reactant enrichment, and mass transport regulation in carbon materials (Figure 8A).

In HCSs, curvature-induced strain distorted the graphene layers and induced π-electron redistribution from the inner concave surface to the outer convex surface, leading to electron-deficient inner surfaces and electron-enriched outer surfaces [138,139]. XPS results showed that, with increasing surface curvature from Ru@HCSs-s to Ru@HCSs-l (curvature increased from low to high), the binding energy of Ru^0 gradually increased (461.71, 462.05, and 462.19 eV; Figure 8B), indicating that higher curvature promoted stronger electron transfer and led to a further decrease in the electron density of Ru NP. This decrease in electron density weakened the interaction between Ru and levulinic acid, as its electron-withdrawing carbonyl and carboxyl groups preferentially interacted with electron-rich metal sites, thereby suppressing its adsorption and hindering the reaction [140].

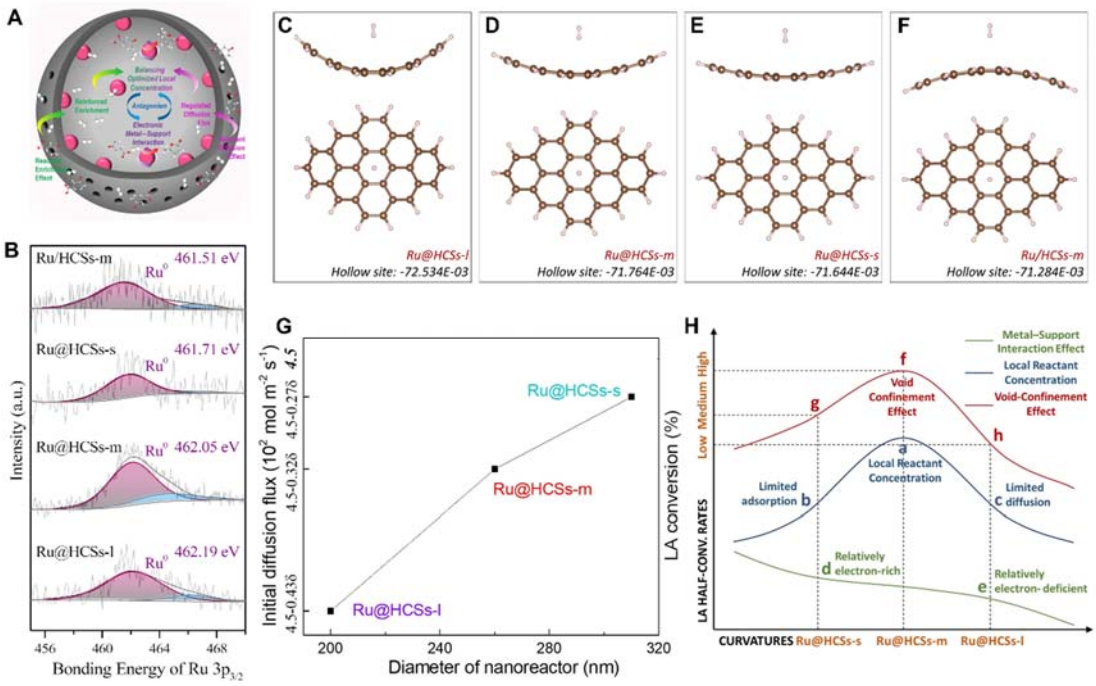

Figure 8. Confinement effect of hollow carbon spheres in enhancing levulinic acid hydrogenation [137]. (A) Schematic illustration of the confinement effect in hollow carbon spheres. (B) XPS survey spectrum of Ru $3p_{3/2}$ bonding energies for Ru/HCSs-m, Ru@HCSs-s, Ru@HCSs-m, and Ru@HCSs-l. (C-F) Optimized configurations of H_2 adsorption on $C_{30}H_{14}$ layers with varying curvatures (G) Initial diffusion fluxes of levulinic acid over Ru@HCSs-s, Ru@HCSs-m, and Ru@HCSs-l. (H) Proposed mechanism for the formation of the confinement effect.

Based on a simplified theoretical model of a curved $C_{30}H_{14}$ layer for H_2 adsorption, calculations showed that among three representative sites (bridge, hollow, and surface), higher curvature consistently led to stronger H_2 adsorption regardless of the adsorption site, while adsorption on the outer surface exhibited the lowest adsorption energy (Figure 8C–F). These results indicated that increasing curvature enhanced reactant enrichment. In contrast, the initial diffusion flux decreased markedly with increasing curvature, indicating inhibited diffusion of levulinic acid (Figure 8G). The interplay between these opposing effects ultimately led to a parabolic relationship between curvature and the apparent reaction rate (Figure 8H). This study advanced the understanding of this effect evolved from an initially ambiguous empirical observation to a systematic elucidation of its underlying mechanisms, enabling its rational and controllable design.

Building on the above mechanistic understanding, constructing carbon materials with tunable confinement structures became an effective strategy to enhance catalytic performance. Among various approaches, metal-organic frameworks (MOFs), composed of metal ions or clusters periodically coordinated with organic ligands to form three-dimensional porous architectures, were demonstrated to be ideal sacrificial templates for deriving carbon materials via pyrolysis [141,142]. The ordered arrangement of metal nodes and ligands effectively suppressed metal aggregation during pyrolysis, enabling the formation of highly dispersed, even atomically dispersed metal species [143]. Moreover, the tunable ligands and framework topology allowed precise control over pore structure (micro/mesopores), surface area, and morphology, facilitating the construction of well-defined confined spaces [144,145]. Meanwhile, the MOF-derived process enabled heteroatom doping (e.g., N, O) and promoted the formation of metal-carbon interfaces, thereby tuning the electronic structure and strengthening metal-support interactions [146]. Consequently, MOF-derived carbons offered superior structural controllability compared to conventional precursors and were more conducive to the synergistic regulation of active metal structures and catalytic microenvironments, leading to enhanced catalytic performance. Li et al. [147] constructed multi-core-shell Co@C-N catalysts via direct pyrolysis of hollow Zn/Co-ZIF precursors. The porous C-N shells facilitated mass transport, while the C-N nanosheets stabilized small Co NPs and modulated their electronic structure. The synergy between structural features and electronic effects led to excellent catalytic performance in aerobic oxidation of alcohols. Moreover, the pyrolysis temperature played a crucial role in regulating the catalyst structure. At low temperatures, the MOF precursor was insufficiently carbonized, resulting in weak interactions

between Co species and C-N nanosheets. In contrast, excessively high temperatures (e.g., above 900 °C) led to severe Co aggregation (particle sizes exceeding 100 nm), with some NPs migrating to the outer shell, accompanied by a decrease in total nitrogen content. Therefore, precise control of the pyrolysis temperature was essential for achieving the synergistic optimization of metal dispersion, interfacial interactions, and microenvironment structure. Similarly, Luo et al. [148] constructed nanocage structures by pyrolyzing ZIF-8@ZIF-67 at 920 °C, achieving an ultrahigh Co loading (>30 wt%) while maintaining excellent dispersion and a narrow particle size distribution. The porous channels and hollow architecture facilitated the diffusion of reactants and hydrocarbon products, thereby enhancing C_5^+ selectivity and CO conversion.

Overall, MOF-derived carbon materials could effectively achieve the synergistic optimization of metal dispersion, electronic structure, and catalytic microenvironment, exhibiting superior performance compared to conventional carbon precursors in various reactions. However, compared with traditional carbon materials, MOF-derived systems still faced several practical challenges [149,150]: their structures strongly depended on the precursor and pyrolysis conditions, leading to limited reproducibility and controllability; high-temperature treatment often induced metal aggregation and the loss of heteroatoms (e.g., N), thereby weakening interfacial interactions; moreover, the relatively high cost and complex synthesis of MOF precursors hindered large-scale application. Despite these limitations, MOF-derived carbons retained unique advantages in structural tunability and multifunctional integration, providing an important platform for the synergistic regulation of structure and microenvironments of active sites, and thus held considerable potential for future development.

6. Conclusion and Outlook

Carbon-based materials, featuring high structural tunability, enable multilevel regulation in thermocatalysis. They allow precise tuning of active metal structures through meta-support interactions, heteroatom doping, and spatial confinement, while their pore and layered architectures facilitate controlled mass transport and adsorption. Moreover, modulation of surface wettability and interfacial polarity enables the construction of favorable reaction microenvironments, leading to enhanced activity, selectivity, and stability. Importantly, the synergistic regulation of active metal structures and the surrounding microenvironment can further optimize catalytic performance.

Despite these advances, several key challenges currently limit the development of carbon-based materials in thermocatalysis:

(1) Carbon-based materials, despite their high thermal and chemical stability, diverse surface chemistry, and favorable mass transport properties, often face a trade-off between catalytic activity and stability under practical thermocatalytic conditions.

(2) The intrinsically heterogeneous and dynamically evolving surfaces of carbon supports hinder precise structural control and unambiguous identification of active sites, while current characterization techniques remain insufficient to fully resolve structure-activity relationships under reaction conditions.

(3) Theoretical descriptions of metal-carbon interfaces often oversimplify carbon supports as idealized surfaces, neglecting defects, dopants, edge structures, and sp^2/sp^3 heterogeneity, which leads to discrepancies between theoretical predictions and experimental observations.

To address the above challenges, several research directions should be explored in future studies:

(1) To achieve the integration of high activity and stability, the design of carbon-based catalysts should emphasize the synergy among structural regulation, interfacial optimization, and microenvironment engineering. On the one hand, the structure and coordination environment of active metal sites can be precisely tuned via defect engineering, heteroatom doping, and confinement strategies, thereby increasing site exposure and modulating electronic properties to enhance the activation of key intermediates. On the other hand, tailoring the surrounding microenvironment (e.g., surface wettability, local polarity, and pore architecture) can optimize reactant enrichment, mass transport, and intermediate adsorption/desorption, lowering energy barriers and suppressing side reactions, thereby stabilizing highly active sites and achieving a synergy between catalytic activity and long-term stability.

(2) Future research should focus on developing synthetic strategies for well-defined carbon structures, such as controllable defect engineering, heteroatom configuration regulation, and atomically dispersed metal-carbon coordination environments. Meanwhile, advanced *in situ/operando* characterization techniques (e.g., *operando* XAS, DRIFTS, Raman spectroscopy, and *in situ/operando* TEM) combined with kinetic analysis are essential to track the dynamic evolution of catalytic sites

and establish reliable structure-activity relationships under realistic reaction conditions.

(3) To bridge the gap between theoretical predictions and experiments, future theoretical studies should adopt more realistic models of carbon materials, incorporating defects, heteroatom dopants, edge structures, and sp^2/sp^3 heterogeneity. Integrating multiscale modeling with machine-learning-assisted simulations may further improve the predictive capability for metal-carbon interfaces.

Author Contributions: Q.L.: Investigation, Writing—original draft, and Visualization. L.L.: Conceptualization, Writing—review & editing, and Supervision. Y.C., Z.M., H.W., A.W. and L.W.: Formal analysis and investigation. All authors have read and agreed to the published version of the manuscript.

Acknowledgments: This work was supported by the Fundamental Research Funds for the Central Universities (No. 226-2024-00225 and 226-2025-00175), the National Natural Science Foundation of China (No. 22572168 and 22202176), the Science and Technology Breakthrough project of the Inner Mongolia Autonomous Region (No. 2025KJTW0007), the Inner Mongolia Science and Technology Innovation Development Special Fund and Daqingshan Laboratory Scientific and Technological Support Program (No. 2025KYPT0190), and the Key Research and Development Program of Zhejiang Province (Grant No. 2025C01176).

Conflicts of Interest: The authors declare no conflicts of interest.

References

[1] Bai, H.; Li, C.; Shi, G. Functional Composite Materials Based on Chemically Converted Graphene. *Adv. Mater.* **2011**, *23*, 1089–1115, doi:10.1002/adma.201003753.

[2] Li, T.; Li, H.; Li, C. Progress in Effects of Microenvironment of Carbon-based Catalysts on Hydrodeoxygenation of Biomass. *ChemCatChem* **2021**, *13*, 1074–1088, doi:10.1002/cctc.202001369.

[3] Varma, R.S. Biomass-Derived Renewable Carbonaceous Materials for Sustainable Chemical and Environmental Applications. *ACS Sustain. Chem. Eng.* **2019**, *7*, 6458–6470, doi:10.1021/acssuschemeng.8b06550.

[4] Bachleitner, S.; Ata, Ö.; Mattanovich, D. The Potential of CO_2-Based Production Cycles in Biotechnology to Fight the Climate Crisis. *Nat. Commun.* **2023**, *14*, 6978, doi:10.1038/s41467-023-42790-6.

[5] Yao, D.; Yang, H.; Hu, Q.; Chen, Y.; Chen, H.; Williams, P.T. Carbon Nanotubes from Post-Consumer Waste Plastics: Investigations into Catalyst Metal and Support Material Characteristics. *Appl. Catal. B Environ.* **2021**, *280*, 119413, doi:10.1016/j.apcatb.2020.119413.

[6] Zhao, C.; Yan, J.; Tian, X.; Xue, X.; Zhao, Y. Progress in Thermal Energy Storage Technologies for Achieving Carbon Neutrality. *Carbon Neutrality* **2023**, *2*, 10, doi:10.1007/s43979-023-00050-y.

[7] Huang, G.; Lu, Y.; Zhao, X.; Baxtiyarovich, A.F.; Oleszczuk, P.; Wiśniewska, M.; et al. Biochar-Based Low-Carbon Construction Materials. *Net Zero* **2025**, *1*, 1-5.

[8] Wang, L.; Wang, L.; Meng, X.; Xiao, F. New Strategies for the Preparation of Sinter-Resistant Metal-Nanoparticle-Based Catalysts. *Adv. Mater.* **2019**, *31*, 1901905, doi:10.1002/adma.201901905.

[9] Gerber, I.C.; Serp, P. A Theory/Experience Description of Support Effects in Carbon-Supported Catalysts. *Chem. Rev.* **2020**, *120*, 1250–1349, doi:10.1021/acs.chemrev.9b00209.

[10] Arora, S.; Gupta, N.; Singh, V. Improved Pd/Ru Metal Supported Graphene Oxide Nano-Catalysts for Hydrodeoxygenation (HDO) of Vanillyl Alcohol, Vanillin and Lignin. *Green Chem.* **2020**, *22*, 2018–2027, doi:10.1039/D0GC00052C.

[11] Yin, P.; Yan, Q.; Liang, H. Strong Metal-Support Interactions through Sulfur-Anchoring of Metal Catalysts on Carbon Supports. *Angew. Chem.* **2023**, *135*, e202302819, doi:10.1002/ange.202302819.

[12] Baker, L.R.; Kennedy, G.; Van Spronsen, M.; Hervier, A.; Cai, X.; Chen, S.; et al. Furfuraldehyde Hydrogenation on Titanium Oxide-Supported Platinum Nanoparticles Studied by Sum Frequency Generation Vibrational Spectroscopy: Acid–Base Catalysis Explains the Molecular Origin of Strong Metal–Support Interactions. *J. Am. Chem. Soc.* **2012**, *134*, 14208–14216, doi:10.1021/ja306079h.

[13] Xu, M.; Peng, M.; Tang, H.; Zhou, W.; Qiao, B.; Ma, D. Renaissance of Strong Metal–Support Interactions. *J. Am. Chem. Soc.* **2024**, *146*, 2290–2307, doi:10.1021/jacs.3c09102.

[14] Zhang, J.; Wang, H.; Wang, L.; Ali, S.; Wang, C.; Wang, L.; et al. Wet-Chemistry Strong Metal–Support Interactions in Titania-Supported Au Catalysts. *J. Am. Chem. Soc.* **2019**, *141*, 2975–2983,

doi:10.1021/jacs.8b10864.

[15] Gangarajula, Y.; Hong, F.; Li, Q.; Jiang, X.; Liu, W.; Akri, M.; et al. Operando Induced Strong Metal-Support Interaction of Rh/CeO_2 Catalyst in Dry Reforming of Methane. *Appl. Catal. B Environ.* **2024**, *343*, 123503, doi:10.1016/j.apcatb.2023.123503.

[16] Yu, J.; Qin, X.; Yang, Y.; Lv, M.; Yin, P.; Wang, L.; et al. Highly Stable Pt/CeO_2 Catalyst with Embedding Structure toward Water–Gas Shift Reaction. *J. Am. Chem. Soc.* **2024**, *146*, 1071–1080, doi:10.1021/jacs.3c12061.

[17] Liu, J.; Wang, L.; Okejiri, F.; Luo, J.; Zhao, J.; Zhang, P.; et al. Deep Understanding of Strong Metal Interface Confinement: A Journey of Pd/FeO_x Catalysts. *ACS Catal.* **2020**, *10*, 8950–8959, doi:10.1021/acscatal.0c01447.

[18] Wu, P.; Tan, S.; Moon, J.; Yan, Z.; Fung, V.; Li, N.; et al. Harnessing Strong Metal–Support Interactions via a Reverse Route. *Nat. Commun.* **2020**, *11*, 3042, doi:10.1038/s41467-020-16674-y.

[19] Wang, H.; Wang, L.; Lin, D.; Feng, X.; Niu, Y.; Zhang, B.; et al. Strong Metal–Support Interactions on Gold Nanoparticle Catalysts Achieved through Le Chatelier's Principle. *Nat. Catal.* **2021**, *4*, 418–424, doi:10.1038/s41929-021-00611-3.

[20] Zhang, K.; Wang, H.; Tang, R.; Huang, Y.; Lv, Y.; Wu, H.; et al. Stable and Selective CO_2 Hydrogenation over the Supported Rh Catalyst Modified with Titanium Oxide Overlayers. *ACS Catal.* **2025**, *15*, 19840–19849, doi:10.1021/acscatal.5c05575.

[21] Jiang, Z.-S.; Zhao, Y.-H.; Huang, C.-F.; Song, Y.-H.; Li, D.-P.; Liu, Z.-T.; et al. Metal-Support Interactions Regulated via Carbon Coating – A Case Study of Co/SiO2 for Fischer-Tropsch Synthesis. *Fuel* **2018**, *226*, 213–220, doi:10.1016/j.fuel.2018.03.195.

[22] Dai, J.; Sun, Y.; Liu, Z.; Zhang, Y.; Duan, S.; Wang, R. Using *In Situ* Transmission Electron Microscopy to Study Strong Metal-Support Interactions in Heterogeneous Catalysis. *Angew. Chem. Int. Ed.* **2024**, e202409673, doi:10.1002/anie.202409673.

[23] Zhang, J.; Wang, M.; Gao, Z.; Qin, X.; Xu, Y.; Wang, Z.; et al. Importance of Species Heterogeneity in Supported Metal Catalysts. *J. Am. Chem. Soc.* **2022**, *144*, 5108–5115, doi:10.1021/jacs.2c00202.

[24] Dong, C.; Gao, Z.; Li, Y.; Peng, M.; Wang, M.; Xu, Y.; et al. Fully Exposed Palladium Cluster Catalysts Enable Hydrogen Production from Nitrogen Heterocycles. *Nat. Catal.* **2022**, *5*, 485–493, doi:10.1038/s41929-022-00769-4.

[25] Li, X.-H.; Antonietti, M. Metal Nanoparticles at Mesoporous N-Doped Carbons and Carbon Nitrides: Functional Mott–Schottky Heterojunctions for Catalysis. *Chem. Soc. Rev.* **2013**, *42*, 6593, doi:10.1039/c3cs60067j.

[26] Jagadeesh, R.V.; Surkus, A.-E.; Junge, H.; Pohl, M.-M.; Radnik, J.; Rabeah, J.; et al. Nanoscale Fe_2O_3 -Based Catalysts for Selective Hydrogenation of Nitroarenes to Anilines. *Science* **2013**, *342*, 1073–1076, doi:10.1126/science.1242005.

[27] Zhang, Y.; Peng, X.; Tian, H.-R.; Yang, B.; Chen, Z.-C.; Li, J.; et al. Fullerene on Non-Iron Cluster-Matrix Co-Catalysts Promotes Collaborative H2 and N2 Activation for Ammonia Synthesis. *Nat. Chem.* **2024**, *16*, 1781–1787, doi:10.1038/s41557-024-01626-6.

[28] Zheng, J.; Huang, L.; Cui, C.-H.; Chen, Z.-C.; Liu, X.-F.; Duan, X.; et al. Ambient-Pressure Synthesis of Ethylene Glycol Catalyzed by C_{60} -Buffered Cu/SiO_2. *Science* **2022**, *376*, 288–292, doi:10.1126/science.abm9257.

[29] Liu, L.; Lu, J.; Liu, M.; Wang, H.; Zhang, J.; Xu, G.; et al. Copper Nanoparticles Stabilized by Adjacent Methyl Groups on Silica for Durable Catalysts. *CCS Chem.* **2025**, 1–12, doi:10.31635/ccschem.025.202505638.

[30] Hong, J.; Wang, B.; Xiao, G.; Wang, N.; Zhang, Y.; Khodakov, A.Y.; et al. Tuning the Metal–Support Interaction and Enhancing the Stability of Titania-Supported Cobalt Fischer–Tropsch Catalysts via Carbon Nitride Coating. *ACS Catal.* **2020**, *10*, 5554–5566, doi:10.1021/acscatal.0c01121.

[31] Wang, D.; Wang, Z.; Xiong, J.; Yu, Z.; Lu, X. Metal Stabilization of Metal-Supported Catalysts: Anchoring Strategies and Catalytic Applications in Carbon Resources Conversion. *ChemCatChem* **2025**, *17*, e00182, doi:10.1002/cctc.202500182.

[32] Luo, Q.; Wang, H.; Lv, Y.; Fan, J.; Wu, H.; Fang, W.; et al. Hydrophobic Poly(Divinylbenzene) Polymer-Supported Ruthenium Catalysts for Efficient Hydrogenation of Pyridines in Water. *Angew. Chem. Int. Ed.* **2025**, *64*, e202510284, doi:10.1002/anie.202510284.

[33] Wang, H.; Li, H.; Duan, J.; Wang, L.; Xiao, F.-S. Adjustment of Molecular Sorption Equilibrium on Catalyst Surface for Boosting Catalysis. *Acc. Chem.*

Res. **2025**, *58*, 440–451, doi:10.1021/acs.accounts.4c00713.

[34] Zhu, Z.-S.; Zhong, S.; Cheng, C.; Zhou, H.; Sun, H.; Duan, X.; et al. Microenvironment Engineering of Heterogeneous Catalysts for Liquid-Phase Environmental Catalysis. *Chem. Rev.* **2024**, *124*, 11348–11434, doi:10.1021/acs.chemrev.4c00276.

[35] Jiao, L.; Wang, J.; Jiang, H.-L. Microenvironment Modulation in Metal–Organic Framework-Based Catalysis. *Acc. Mater. Res.* **2021**, *2*, 327–339, doi:10.1021/accountsmr.1c00009.

[36] Teimouri, Z.; Nanda, S.; Abatzoglou, N.; Dalai, A.K. Application of Activated Carbon in Renewable Energy Conversion and Storage Systems: A Review. *Environ. Chem. Lett.* **2024**, *22*, 1073–1092, doi:10.1007/s10311-023-01690-3.

[37] Li, N.; Ma, X.; Zha, Q.; Kim, K.; Chen, Y.; Song, C. Maximizing the Number of Oxygen-Containing Functional Groups on Activated Carbon by Using Ammonium Persulfate and Improving the Temperature-Programmed Desorption Characterization of Carbon Surface Chemistry. *Carbon* **2011**, *49*, 5002–5013, doi:10.1016/j.carbon.2011.07.015.

[38] Hamood Ur Rehman, M.; Hussain, M.; Zidi, C.; Akhter, P.; Jamil, F.; Majeed, K.; et al. Eco-Friendly Biodiesel Synthesis via Microbubble-Aided Transesterification and Leaf-Derived Green Carbon Catalyst. *Korean J. Chem. Eng.* **2026**, *43*, 179–194, doi:10.1007/s11814-025-00558-2.

[39] Rahman, G.; Najaf, Z.; Mehmood, A.; Bilal, S.; Shah, A.; Mian, S.; et al. An Overview of the Recent Progress in the Synthesis and Applications of Carbon Nanotubes. *C* **2019**, *5*, 3, doi:10.3390/c5010003.

[40] Yadav, M.D.; Joshi, H.M.; Sawant, S.V.; Dasgupta, K.; Patwardhan, A.W.; Joshi, J.B. Advances in the Application of Carbon Nanotubes as Catalyst Support for Hydrogenation Reactions. *Chem. Eng. Sci.* **2023**, *272*, 118586, doi:10.1016/j.ces.2023.118586.

[41] Setaro, A.; Adeli, M.; Glaeske, M.; Przyrembel, D.; Bisswanger, T.; Gordeev, G.; et al. Preserving π-Conjugation in Covalently Functionalized Carbon Nanotubes for Optoelectronic Applications. *Nat. Commun.* **2017**, *8*, 14281, doi:10.1038/ncomms14281.

[42] Xu, J.; Yao, Y.; Zhu, C.; Fang, Q.; Song, S.; Chen, B.; et al. Curved Strain-Induced Modulation of Potential Difference Optimizes Electron-Mediated Persulfate Activation for Pollutant Removal. *Appl. Catal. B Environ. Energy* **2024**, *357*, 124285, doi:10.1016/j.apcatb.2024.124285.

[43] Pan, X.; Bao, X. The Effects of Confinement inside Carbon Nanotubes on Catalysis. *Acc. Chem. Res.* **2011**, *44*, 553–562, doi:10.1021/ar100160t.

[44] Dai, J.; Zhang, H. Recent Advances in Catalytic Confinement Effect within Micro/Meso-Porous Crystalline Materials. *Small* **2021**, *17*, 2005334, doi:10.1002/smll.202005334.

[45] Qiu, B.; Xing, M.; Zhang, J. Recent Advances in Three-Dimensional Graphene Based Materials for Catalysis Applications. *Chem. Soc. Rev.* **2018**, *47*, 2165–2216, doi:10.1039/C7CS00904F.

[46] Zhuo, H.-Y.; Zhang, X.; Liang, J.-X.; Yu, Q.; Xiao, H.; Li, J. Theoretical Understandings of Graphene-Based Metal Single-Atom Catalysts: Stability and Catalytic Performance. *Chem. Rev.* **2020**, *120*, 12315–12341, doi:10.1021/acs.chemrev.0c00818.

[47] Huang, F.; Peng, M.; Liu, H.; Ma, D. Atomically Dispersed Metals on Nanodiamond-Derived Hybrid Materials for Heterogeneous Catalysis. *Acc. Mater. Res.* **2023**, *4*, 223–236, doi:10.1021/accountsmr.2c00152.

[48] Liu, C.; Li, Q.; Kang, W.; Lei, W.; Wang, X.; Lu, C.; et al. Structural Design and Mechanism Analysis of Hierarchical Porous Carbon Fibers for Advanced Energy and Environmental Applications. *J. Mater. Chem. A* **2022**, *10*, 10–49, doi:10.1039/D1TA08646D.

[49] Gao, C.; Lyu, F.; Yin, Y. Encapsulated Metal Nanoparticles for Catalysis. *Chem. Rev.* **2021**, *121*, 834–881, doi:10.1021/acs.chemrev.0c00237.

[50] Hu, B.; Zhao, D.; Tian, B.; Chen, C.; Zou, Z. Pressure-Enhanced Electrocatalysis for Small-Molecule Conversion. *Energy Mater. Adv.* **2025**, *6*, 0359, doi:10.34133/energymatadv.0359.

[51] Zhai, Y.; Zhu, Z.; Dong, S. Carbon-Based Nanostructures for Advanced Catalysis. *ChemCatChem* **2015**, *7*, 2806–2815, doi:10.1002/cctc.201500323.

[52] Chen, Y.; Wei, J.; Duyar, M.S.; Ordomsky, V.V.; Khodakov, A.Y.; Liu, J. Carbon-Based Catalysts for Fischer–Tropsch Synthesis. *Chem. Soc. Rev.* **2021**, *50*, 2337–2366, doi:10.1039/D0CS00905A.

[53] Kumar, S.; Kaur, P.; Hsu, C.-Y.; Mustafa, M.A.; Rani, J.; Kaur, J.; et al. Advances in Surface Modification of Biomass and Its Nanostructuring for Enhanced Environmental Remediation Applications. *Mater. Adv.*

2025, *6*, 8774–8815, doi:10.1039/D5MA00494B.

[54] Huang, Y.; Chen, Y.; Xu, M.; Asset, T.; Tieu, P.; Gili, A.; et al. Catalysts by Pyrolysis: Direct Observation of Chemical and Morphological Transformations Leading to Transition Metal-Nitrogen-Carbon Materials. *Mater. Today* **2021**, *47*, 53–68, doi:10.1016/j.mattod.2021.02.006.

[55] Hu, X.; Yang, B.; Ke, S.; Liu, Y.; Fang, M.; Huang, Z.; et al. Review and Perspectives of Carbon-Supported Platinum-Based Catalysts for Proton Exchange Membrane Fuel Cells. *Energy Fuels* **2023**, *37*, 11532–11566, doi:10.1021/acs.energyfuels.3c01265.

[56] Huo, J.; Tessonnier, J.-P.; Shanks, B.H. Improving Hydrothermal Stability of Supported Metal Catalysts for Biomass Conversions: A Review. *ACS Catal.* **2021**, *11*, 5248–5270, doi:10.1021/acscatal.1c00197.

[57] Ding, X.; Zhu, M.; Sun, B.; Yang, Z.; Han, Y.-F. An Overview on Dynamic Phase Transformation and Surface Reconstruction of Iron Catalysts for Catalytic Hydrogenation of CO_x for Hydrocarbons. *ACS Catal.* **2024**, *14*, 6137–6168, doi:10.1021/acscatal.3c05854.

[58] Yang, H.; Duan, P.; Zhuang, Z.; Luo, Y.; Shen, J.; Xiong, Y.; et al. Understanding the Dynamic Evolution of Active Sites among Single Atoms, Clusters, and Nanoparticles. *Adv. Mater.* **2025**, *37*, 2415265, doi:10.1002/adma.202415265.

[59] Lin, L.; Yao, S.; Gao, R.; Liang, X.; Yu, Q.; Deng, Y.; et al. A Highly CO-Tolerant Atomically Dispersed Pt Catalyst for Chemoselective Hydrogenation. *Nat. Nanotechnol.* **2019**, *14*, 354–361, doi:10.1038/s41565-019-0366-5.

[60] Wang, F.; Liu, Z.; Xiang, Z.; Zhang, C.; Lu, A.; Qi, F.; et al. Delocalized C S Decorates a 3D Sp^2 -Hybridized Carbon Skeleton for Superior Charge Transfer Kinetics of Anodes. *Energy Environ. Sci.* **2023**, *16*, 5154–5169, doi:10.1039/D3EE01493B.

[61] Tao, L.; Wang, Y.; Zou, Y.; Zhang, N.; Zhang, Y.; Wu, Y.; et al. Charge Transfer Modulated Activity of Carbon-Based Electrocatalysts. *Adv. Energy Mater.* **2020**, *10*, 1901227, doi:10.1002/aenm.201901227.

[62] Zhu, J.; Holmen, A.; Chen, D. Carbon Nanomaterials in Catalysis: Proton Affinity, Chemical and Electronic Properties, and Their Catalytic Consequences. *ChemCatChem* **2013**, *5*, 378–401, doi:10.1002/cctc.201200471.

[63] Liu, L.; Corma, A. Metal Catalysts for Heterogeneous Catalysis: From Single Atoms to Nanoclusters and Nanoparticles. *Chem. Rev.* **2018**, *118*, 4981–5079, doi:10.1021/acs.chemrev.7b00776.

[64] Zhang, J.; Yu, S.; Liu, X.; Wang, M.; Gao, Z.; Qin, X.; et al. Interplay Between Metal and Acid Sites Tunes the Catalytic Selectivity Over Pd/Nanodiamond Catalysts. *J. Am. Chem. Soc.* **2024**, *146*, 34990–34997, doi:10.1021/jacs.4c15099.

[65] Li, J.; Chen, W.; Zhao, H.; Zheng, X.; Wu, L.; Pan, H.; et al. Size-Dependent Catalytic Activity over Carbon-Supported Palladium Nanoparticles in Dehydrogenation of Formic Acid. *J. Catal.* **2017**, *352*, 371–381, doi:10.1016/j.jcat.2017.06.007.

[66] Yang, Y.; Yang, Y.; Pei, Z.; Wu, K.-H.; Tan, C.; Wang, H.; et al. Recent Progress of Carbon-Supported Single-Atom Catalysts for Energy Conversion and Storage. *Matter* **2020**, *3*, 1442–1476, doi:10.1016/j.matt.2020.07.032.

[67] Wang, S.; Li, J.; Li, Q.; Bai, X.; Wang, J. Metal Single-Atom Coordinated Graphitic Carbon Nitride as an Efficient Catalyst for CO Oxidation. *Nanoscale* **2020**, *12*, 364–371, doi:10.1039/C9NR07726J.

[68] Gawande, M.B.; Fornasiero, P.; Zbořil, R. Carbon-Based Single-Atom Catalysts for Advanced Applications. *ACS Catal.* **2020**, *10*, 2231–2259, doi:10.1021/acscatal.9b04217.

[69] Li, L.; Zhu, Z.H.; Yan, Z.F.; Lu, G.Q.; Rintoul, L. Catalytic Ammonia Decomposition over Ru/Carbon Catalysts: The Importance of the Structure of Carbon Support. *Appl. Catal. Gen.* **2007**, *320*, 166–172, doi:10.1016/j.apcata.2007.01.029.

[70] Wang, L.; Wang, D.; Li, Y. Single-atom Catalysis for Carbon Neutrality. *Carbon Energy* **2022**, *4*, 1021–1079, doi:10.1002/cey2.194.

[71] Yang, X.-F.; Wang, A.; Qiao, B.; Li, J.; Liu, J.; Zhang, T. Single-Atom Catalysts: A New Frontier in Heterogeneous Catalysis. *Acc. Chem. Res.* **2013**, *46*, 1740–1748, doi:10.1021/ar300361m.

[72] Sui, C.; Ma, H.; Huang, F.; Wang, M.; Cai, X.; Diao, J.; et al. Fully Exposed Nickel Clusters for Semihydrogenation of Acetylene. *ACS Catal.* **2024**, *14*, 14689–14695, doi:10.1021/acscatal.4c04462.

[73] Yang, F.; Deng, D.; Pan, X.; Fu, Q.; Bao, X. Understanding Nano Effects in Catalysis. *Natl. Sci. Rev.* **2015**, *2*, 183–201, doi:10.1093/nsr/nwv024.

[74] Chen, W.; Pan, X.; Bao, X. Tuning of Redox Properties of Iron and Iron Oxides via Encapsulation within Carbon Nanotubes. *J. Am. Chem. Soc.* **2007**, *129*,

7421–7426, doi:10.1021/ja0713072.

[75] Xiao, J.; Pan, X.; Guo, S.; Ren, P.; Bao, X. Toward Fundamentals of Confined Catalysis in Carbon Nanotubes. *J. Am. Chem. Soc.* **2015**, *137*, 477–482, doi:10.1021/ja511498s.

[76] Zhai, P.; Li, Y.; Wang, M.; Liu, J.; Cao, Z.; Zhang, J.; et al. Development of Direct Conversion of Syngas to Unsaturated Hydrocarbons Based on Fischer-Tropsch Route. *Chem* **2021**, *7*, 3027–3051, doi:10.1016/j.chempr.2021.08.019.

[77] Chen, W.; Fan, Z.; Pan, X.; Bao, X. Effect of Confinement in Carbon Nanotubes on the Activity of Fischer−Tropsch Iron Catalyst. *J. Am. Chem. Soc.* **2008**, *130*, 9414–9419, doi:10.1021/ja8008192.

[78] Fei, X.; Wang, P.; Zhang, D.; Wang, H.; Wu, Z. Confined Catalysts Application in Environmental Catalysis: Current Research Progress and Future Prospects. *ChemCatChem* **2021**, *13*, 2313–2336, doi:10.1002/cctc.202001578.

[79] Sheng, Y.; Peng, J.; Ma, L.; Zhang, Y.; Jiang, T.; Li, X. Nickel Nanoparticles Embedded in Porous Carbon-Coated Honeycomb Ceramics: A Potential Monolithic Catalyst for Continuous Hydrogenation Reaction. *Carbon* **2022**, *197*, 171–182, doi:10.1016/j.carbon.2022.06.017.

[80] Yu, H.; Zhang, L.; Gao, S.; Wang, H.; He, Z.; Xu, Y.; et al. In Situ Encapsulated Ultrafine Pd Nanoparticles in Nitrogen-Doped Porous Carbon Derived from Hyper-Crosslinked Polymers Effectively Catalyse Hydrogenation. *J. Catal.* **2021**, *396*, 342–350, doi:10.1016/j.jcat.2021.03.002.

[81] Zhu, Q.-L.; Xu, Q. Immobilization of Ultrafine Metal Nanoparticles to High-Surface-Area Materials and Their Catalytic Applications. *Chem* **2016**, *1*, 220–245, doi:10.1016/j.chempr.2016.07.005.

[82] Zhang, W.; Zhu, K.; Ren, W.; He, H.; Liang, H.; Zhai, Y.; et al. Recent Advances in the Marriage of Catalyst Nanoparticles and Mesoporous Supports. *Adv. Mater. Interfaces* **2022**, *9*, 2101528, doi:10.1002/admi.202101528.

[83] Wu, T.; Lin, J.; Cheng, Y.; Tian, J.; Wang, S.; Xie, S.; et al. Porous Graphene-Confined Fe–K as Highly Efficient Catalyst for CO_2 Direct Hydrogenation to Light Olefins. *ACS Appl. Mater. Interfaces* **2018**, *10*, 23439–23443, doi:10.1021/acsami.8b05411.

[84] Sun, Z.; Sun, B.; Qiao, M.; Wei, J.; Yue, Q.; Wang, C.; et al. A General Chelate-Assisted Co-Assembly to Metallic Nanoparticles-Incorporated Ordered Mesoporous Carbon Catalysts for Fischer–Tropsch Synthesis. *J. Am. Chem. Soc.* **2012**, *134*, 17653–17660, doi:10.1021/ja306913x.

[85] Pan, X.; Fan, Z.; Chen, W.; Ding, Y.; Luo, H.; Bao, X. Enhanced Ethanol Production inside Carbon-Nanotube Reactors Containing Catalytic Particles. *Nat. Mater.* **2007**, *6*, 507–511, doi:10.1038/nmat1916.

[86] Jin, H.; Zhou, K.; Zhang, R.; Cui, H.; Yu, Y.; Cui, P.; et al. Regulating the Electronic Structure through Charge Redistribution in Dense Single-Atom Catalysts for Enhanced Alkene Epoxidation. *Nat. Commun.* **2023**, *14*, 2494, doi:10.1038/s41467-023-38310-1.

[87] Shen, J.; Wu, H.; Sun, W.; Qiao, J.; Cai, H.; Wang, Z.; et al. In-Situ Nitrogen-Doped Hierarchical Porous Hollow Carbon Spheres Anchored with Iridium Nanoparticles as Efficient Cathode Catalysts for Reversible Lithium-Oxygen Batteries. *Chem. Eng. J.* **2019**, *358*, 340–350, doi:10.1016/j.cej.2018.10.038.

[88] Gao, R.; Pan, L.; Lu, J.; Xu, J.; Zhang, X.; Wang, L.; et al. Phosphorus-Doped and Lattice-Defective Carbon as Metal-like Catalyst for the Selective Hydrogenation of Nitroarenes. *ChemCatChem* **2017**, *9*, 4287–4294, doi:10.1002/cctc.201700904.

[89] Cao, Y.; Yu, H.; Tan, J.; Peng, F.; Wang, H.; Li, J.; et al. Nitrogen-, Phosphorous- and Boron-Doped Carbon Nanotubes as Catalysts for the Aerobic Oxidation of Cyclohexane. *Carbon* **2013**, *57*, 433–442, doi:10.1016/j.carbon.2013.02.016.

[90] Yang, M.; Wang, H.; Jin, S.; Zhang, R.; Wang, Y.; Huo, W.; et al. Insight into the Mechanism of Boron-Doping of Carbon Aerogel for Enhancing the Activity of Low-Temperature Selective Catalytic Reduction of NO with NH_3. *Catal. Sci. Technol.* **2021**, *11*, 2057–2072, doi:10.1039/D0CY02006K.

[91] Liu, W.; Zhou, X.; Min, Y.; Huang, J.; Chen, J.; Wu, Y.; et al. Engineering of Local Coordination Microenvironment in Single-Atom Catalysts Enabling Sustainable Conversion of Biomass into a Broad Range of Amines. *Adv. Mater.* **2024**, *36*, 2305924, doi:10.1002/adma.202305924.

[92] Patel, M.A.; Luo, F.; Savaram, K.; Kucheryavy, P.; Xie, Q.; Flach, C.; et al. P and S Dual-Doped Graphitic Porous Carbon for Aerobic Oxidation Reactions: Enhanced Catalytic Activity and Catalytic Sites. *Carbon* **2017**, *114*, 383–392, doi:10.1016/j.carbon.2016.11.064.

[93] Fan, M.; Cui, J.; Wu, J.; Vajtai, R.; Sun, D.; Ajayan, P.M. Improving the Catalytic Activity of Carbon-Supported Single Atom Catalysts by Polynary Metal or Heteroatom Doping. *Small* **2020**, *16*, 1906782, doi:10.1002/smll.201906782.

[94] Peng, X.; Wang, C.; Tan, Z.; Ni, J.; Lin, B.; Lin, J.; et al. N-Induced Electron Transfer Effect on Low-Temperature Activation of Nitrogen for Ammonia Synthesis over Co-Based Catalysts. *ACS Sustain. Chem. Eng.* **2021**, *9*, 1529–1539, doi:10.1021/acssuschemeng.0c05491.

[95] Li, Y.; Xu, Y.; Chen, S.; Shi, X.; Gu, Q.; Wang, L.; et al. Tuning the Electronic Structures of Anchor Sites to Achieve Zero-Valence Single-Atom Catalysts for Advanced Hydrogenation. *Angew. Chem. Int. Ed.* **2024**, *63*, e202406262, doi:10.1002/anie.202406262.

[96] Choi, C.H.; Park, S.H.; Woo, S.I. Phosphorus–Nitrogen Dual Doped Carbon as an Effective Catalyst for Oxygen Reduction Reaction in Acidic Media: Effects of the Amount of P-Doping on the Physical and Electrochemical Properties of Carbon. *J. Mater. Chem.* **2012**, *22*, 12107, doi:10.1039/c2jm31079a.

[97] Zheng, X.; Wu, J.; Cao, X.; Abbott, J.; Jin, C.; Wang, H.; et al. N-, P-, and S-Doped Graphene-like Carbon Catalysts Derived from Onium Salts with Enhanced Oxygen Chemisorption for Zn-Air Battery Cathodes. *Appl. Catal. B Environ.* **2019**, *241*, 442–451, doi:10.1016/j.apcatb.2018.09.054.

[98] Ding, D.; Yang, S.; Qian, X.; Chen, L.; Cai, T. Nitrogen-Doping Positively Whilst Sulfur-Doping Negatively Affect the Catalytic Activity of Biochar for the Degradation of Organic Contaminant. *Appl. Catal. B Environ.* **2020**, *263*, 118348, doi:10.1016/j.apcatb.2019.118348.

[99] Jin, H.; Li, P.; Cui, P.; Shi, J.; Zhou, W.; Yu, X.; et al. Unprecedentedly High Activity and Selectivity for Hydrogenation of Nitroarenes with Single Atomic Co1-N3P1 Sites. *Nat. Commun.* **2022**, *13*, 723, doi:10.1038/s41467-022-28367-9.

[100] McCue, A.J.; Anderson, J.A. Sulfur as a Catalyst Promoter or Selectivity Modifier in Heterogeneous Catalysis. *Catal Sci Technol* **2014**, *4*, 272–294, doi:10.1039/C3CY00754E.

[101] Liu, P.; Qin, R.; Fu, G.; Zheng, N. Surface Coordination Chemistry of Metal Nanomaterials. *J. Am. Chem. Soc.* **2017**, *139*, 2122–2131, doi:10.1021/jacs.6b10978.

[102] Chen, W.; Che, Y.; Xia, J.; Zheng, L.; Lv, H.; Zhang, J.; et al. Metal–Sulfur Interfaces as the Primary Active Sites for Catalytic Hydrogenations. *J. Am. Chem. Soc.* **2024**, jacs.4c02692, doi:10.1021/jacs.4c02692.

[103] Yin, P.; Luo, X.; Ma, Y.; Chu, S.-Q.; Chen, S.; Zheng, X.; et al. Sulfur Stabilizing Metal Nanoclusters on Carbon at High Temperatures. *Nat. Commun.* **2021**, *12*, 3135, doi:10.1038/s41467-021-23426-z.

[104] Liu, L.; Lu, J.; Yang, Y.; Ruettinger, W.; Gao, X.; Wang, M.; et al. Dealuminated Beta Zeolite Reverses Ostwald Ripening for Durable Copper Nanoparticle Catalysts. *Science* **2024**, *383*, 94–101, doi:10.1126/science.adj1962.

[105] Chen, H.; Sholl, D.S. Rapid Diffusion of CH_4 /H_2 Mixtures in Single-Walled Carbon Nanotubes. *J. Am. Chem. Soc.* **2004**, *126*, 7778–7779, doi:10.1021/ja039462d.

[106] Murugesan, K.; Chandrashekhar, V.G.; Kreyenschulte, C.; Beller, M.; Jagadeesh, R.V. A General Catalyst Based on Cobalt Core–Shell Nanoparticles for the Hydrogenation of N-Heteroarenes Including Pyridines. *Angew. Chem. Int. Ed.* **2020**, *59*, 17408–17412, doi:10.1002/anie.202004674.

[107] Bai, L.; Wang, X.; Chen, Q.; Ye, Y.; Zheng, H.; Guo, J.; et al. Explaining the Size Dependence in Platinum-Nanoparticle-Catalyzed Hydrogenation Reactions. *Angew. Chem. Int. Ed.* **2016**, *55*, 15656–15661, doi:10.1002/anie.201609663.

[108] Chen, F.; Li, W.; Sahoo, B.; Kreyenschulte, C.; Agostini, G.; Lund, H.; et al. Hydrogenation of Pyridines Using a Nitrogen-Modified Titania-Supported Cobalt Catalyst. *Angew. Chem.* **2018**, *130*, 14696–14700, doi:10.1002/ange.201803426.

[109] Zhang, S.; Gan, J.; Xia, Z.; Chen, X.; Zou, Y.; Duan, X.; et al. Dual-Active-Sites Design of Co@C Catalysts for Ultrahigh Selective Hydrogenation of N-Heteroarenes. *Chem* **2020**, *6*, 2994–3006, doi:10.1016/j.chempr.2020.07.023.

[110] Dong, C.; Yu, Q.; Ye, R.; Su, P.; Liu, J.; Wang, G. Hollow Carbon Sphere Nanoreactors Loaded with PdCu Nanoparticles: Void-Confinement Effects in Liquid-Phase Hydrogenations. *Angew. Chem. Int. Ed.* **2020**, *59*, 18374–18379, doi:10.1002/anie.202007297.

[111] Kondratyuk, P.; Yates, J.T. Molecular Views of Physical Adsorption Inside and Outside of Single-Wall Carbon Nanotubes. *Acc. Chem. Res.* **2007**, *40*, 995–

1004, doi:10.1021/ar700013c.

[112] Guan, J.; Pan, X.; Liu, X.; Bao, X. Syngas Segregation Induced by Confinement in Carbon Nanotubes: A Combined First-Principles and Monte Carlo Study. *J. Phys. Chem. C* **2009**, *113*, 21687–21692, doi:10.1021/jp906092c.

[113] Luo, Q.; Wang, H.; Xiang, Q.; Lv, Y.; Yang, J.; Song, L.; et al. Polymer-Supported Pd Nanoparticles for Solvent-Free Hydrogenation. *J. Am. Chem. Soc.* **2024**, *146*, 26379–26386, doi:10.1021/jacs.4c09241.

[114] Rahman, M.S.; Barua, A.; Faraezi, S.; Khan, M.S. Role of Surface Oxygen Functional Groups in the Adsorption of Catechol, Hydroquinone, and Aniline on Graphene Oxide. *RSC Adv.* **2025**, *15*, 38211–38217, doi:10.1039/D5RA06051F.

[115] Yang, H.; Yan, R.; Chen, H.; Lee, D.H.; Zheng, C. Characteristics of Hemicellulose, Cellulose and Lignin Pyrolysis. *Fuel* **2007**, *86*, 1781–1788, doi:10.1016/j.fuel.2006.12.013.

[116] Dongil, A.B.; Ghampson, I.T.; García, R.; Fierro, J.L.G.; Escalona, N. Hydrodeoxygenation of Guaiacol over Ni/Carbon Catalysts: Effect of the Support and Ni Loading. *RSC Adv.* **2016**, *6*, 2611–2623, doi:10.1039/C5RA22540J.

[117] Wang, S.; Zhang, M.; Guo, D.; Feng, J.; Pan, H. Construction of Lewis-Brønsted Bifunctional Carbonaceous Acidic Catalyst for Efficient Transformation of Glucose into 5-HMF. *Fuel* **2024**, *363*, 130991, doi:10.1016/j.fuel.2024.130991.

[118] Wang, S.; Hu, R.; Ren, J.; Lv, Y.; Song, L.; Zhao, H.; et al. Surface Hydrophobization of Zeolite Enables Mass Transfer Matching in Gas-Liquid-Solid Three-Phase Hydrogenation under Ambient Pressure. *Nat. Commun.* **2024**, *15*, 2076, doi:10.1038/s41467-024-46505-3.

[119] Hui, Y.; Wang, L.; Xiao, F.-S. Catalysis Enhanced by Catalyst Wettability. *ACS Nano* **2025**, *19*, 7617–7633, doi:10.1021/acsnano.4c18150.

[120] Liu, L.; Zheng, H.; Wu, A.; Li, H.; Cao, A.; Yan, J.; et al. Stabilization of Metal-Based Catalysts for Hydrogenation of CO_2 to C_1 Products. *Energy Fuels* **2025**, *39*, 14483–14499, doi:10.1021/acs.energyfuels.5c03153.

[121] Yu, J.; Chen, W.; Li, K.; Zhang, C.; Li, M.; He, F.; et al. Graphdiyne Nanospheres as a Wettability and Electron Modifier for Enhanced Hydrogenation Catalysis. *Angew. Chem. Int. Ed.* **2022**, *61*, e202207255, doi:10.1002/anie.202207255.

[122] Lin, T.; An, Y.; Yu, F.; Gong, K.; Yu, H.; Wang, C.; et al. Advances in Selectivity Control for Fischer–Tropsch Synthesis to Fuels and Chemicals with High Carbon Efficiency. *ACS Catal.* **2022**, *12*, 12092–12112, doi:10.1021/acscatal.2c03404.

[123] Ha, K.-S.; Kwak, G.; Jun, K.-W.; Hwang, J.; Lee, J. Ordered Mesoporous Carbon Nanochannel Reactors for High-Performance Fischer–Tropsch Synthesis. *Chem. Commun.* **2013**, *49*, 5141, doi:10.1039/c3cc00297g.

[124] Wang, C.; Liu, L.; Li, H.; Wang, L.; Xiao, F.-S. Hydrophobic Catalysts for Syngas Conversion. *Matter* **2023**, *6*, 2697–2710, doi:10.1016/j.matt.2023.05.010.

[125] Liu, Y.; Li, X.; Cheng, Q.; Tian, Y.; Zhang, Y.; Ding, T.; et al. Efficient and Stable Production of Long-Chain Hydrocarbons over Hydrophobic Carbon-Encapsulated TiO_2 -Supported Ru Catalyst in Fischer–Tropsch Synthesis. *ACS Catal.* **2024**, *14*, 10365–10375, doi:10.1021/acscatal.4c02979.

[126] Xu, Y.; Li, X.; Gao, J.; Wang, J.; Ma, G.; Wen, X.; et al. A Hydrophobic FeMn@Si Catalyst Increases Olefins from Syngas by Suppressing C1 By-Products. *Science* **2021**, *371*, 610–613, doi:10.1126/science.abb3649.

[127] Yu, X.; Zhang, J.; Wang, X.; Ma, Q.; Gao, X.; Xia, H.; Lai, X.; Fan, S.; Zhao, T.-S. Fischer-Tropsch Synthesis over Methyl Modified Fe2O3@SiO2 Catalysts with Low CO_2 Selectivity. *Appl. Catal. B Environ.* **2018**, *232*, 420–428, doi:10.1016/j.apcatb.2018.03.048.

[128] Fang, W.; Wang, C.; Liu, Z.; Wang, L.; Liu, L.; Li, H.; et al. Physical Mixing of a Catalyst and a Hydrophobic Polymer Promotes CO Hydrogenation through Dehydration. *Science* **2022**, *377*, 406–410, doi:10.1126/science.abo0356.

[129] Li, H.; Fang, W.; Wang, L.-X.; Liu, Y.; Liu, L.; Sun, T.; et al. Physical Regulation of Copper Catalyst with a Hydrophobic Promoter for Enhancing CO2 Hydrogenation to Methanol. *Innovation* **2023**, *4*, 100445, doi:10.1016/j.xinn.2023.100445.

[130] Xi, J.; Sun, H.; Wang, D.; Zhang, Z.; Duan, X.; Xiao, J.; et al. Confined-Interface-Directed Synthesis of Palladium Single-Atom Catalysts on Graphene/Amorphous Carbon. *Appl. Catal. B Environ.* **2018**, *225*, 291–297, doi:10.1016/j.apcatb.2017.11.057.

[131] Wang, B.; Yao, Y.; Yu, X.; Wang, C.; Wu, C.; Zou, Z.

Understanding the Enhanced Catalytic Activity of High Entropy Alloys: From Theory to Experiment. *J. Mater. Chem. A* **2021**, *9*, 19410–19438, doi:10.1039/D1TA02718B.

[132] Nakaya, Y.; Furukawa, S. Catalysis of Alloys: Classification, Principles, and Design for a Variety of Materials and Reactions. *Chem. Rev.* **2023**, *123*, 5859–5947, doi:10.1021/acs.chemrev.2c00356.

[133] Wang, A.; Ma, Y.; Zhao, D. Pore Engineering of Porous Materials: Effects and Applications. *ACS Nano* **2024**, *18*, 22829–22854, doi:10.1021/acsnano.4c08708.

[134] Zhang, F.; Wang, H.; Liu, X.; Wang, G.; Wang, B. Higher Mechanical Stability and Mutual-Stabilizing/Confining Effect Enables Anti-Pulverization SbSn Alloy/N-Doped Porous Carbon with High-Performance in Sodium-Based Dual-Ion Batteries. *Chem. Eng. J.* **2023**, *475*, 146131, doi:10.1016/j.cej.2023.146131.

[135] Lu, C.; Zhou, S.; Zhou, W.; Zhou, C.; Li, Q.; Zeng, A.; et al. Carbon-Confined Cu-Pd Alloy Nanoparticles as High-Performance Catalysts for Acetylene Selective Hydrogenation. *Chem. Eng. J.* **2023**, *464*, 142609, doi:10.1016/j.cej.2023.142609.

[136] Zhao, X.; Wang, S.; Li, H.; Wei, Y.; Li, Y.; Li, H.; et al. Pt–Fe Bimetallic Nanoparticles Confined in Nitrogen-Doped Carbon Nanoshells as a Catalyst for the Reverse Water–Gas Shift Reaction. *ACS Appl. Nano Mater.* **2025**, *8*, 10315–10325, doi:10.1021/acsanm.5c00722.

[137] Yu, Z.; Ji, N.; Xiong, J.; Li, X.; Zhang, R.; Zhang, L.; et al. Ruthenium-Nanoparticle-Loaded Hollow Carbon Spheres as Nanoreactors for Hydrogenation of Levulinic Acid: Explicitly Recognizing the Void-Confinement Effect. *Angew. Chem. Int. Ed.* **2021**, *60*, 20786–20794, doi:10.1002/anie.202107314.

[138] Haddon, R.C. Chemistry of the Fullerenes: The Manifestation of Strain in a Class of Continuous Aromatic Molecules. *Science* **1993**, *261*, 1545–1550, doi:10.1126/science.261.5128.1545.

[139] Peralta-Inga, Z.; Lane, P.; Murray, J.S.; Boyd, S.; Grice, M.E.; O'Connor, C.J.; et al. Characterization of Surface Electrostatic Potentials of Some (5,5) and (*n* ,1) Carbon and Boron/Nitrogen Model Nanotubes. *Nano Lett.* **2003**, *3*, 21–28, doi:10.1021/nl020222q.

[140] Meng, Z.; Liu, Y.; Yang, G.; Cao, Y.; Wang, H.; Peng, F.; et al. Electron-Rich Ruthenium on Nitrogen-Doped Carbons Promoting Levulinic Acid Hydrogenation to γ-Valerolactone: Effect of Metal–Support Interaction. *ACS Sustain. Chem. Eng.* **2019**, *7*, 16501–16510, doi:10.1021/acssuschemeng.9b03742.

[141] Ipadeola, A.K.; Gamal, A.; Abdullah, A.M.; Haruna, A.B.; Ozoemena, K.I.; Eid, K. Pd Nanocrystals Encapsulated in MOF-Derived Ni/N-Doped Hollow Carbon Nanosheets for Efficient Thermal CO Oxidation: Unveiling the Effect of Porosity. *Catal. Sci. Technol.* **2023**, *13*, 4873–4882, doi:10.1039/D3CY00623A.

[142] Peng, Y.; Bi, P.; Zhu, X.; Liu, P.; Ren, M.; Zu, Y.; et al. Metal–Organic Framework-Derived CoO_X /Co_9 S_8 @NC Nanocomposites Regulated by Oxygen and Sulfur Dual Vacancies as Efficient Trifunctional Electrocatalysts. *Energy Mater. Adv.* **2025**, *6*, 0206, doi:10.34133/energymatadv.0206.

[143] Wang, J.; Sun, H.; Wu, Y.; Hu, H.; Duan, F.; Du, M.; et al. Advances and Perspectives of Mild Thermal Treatment Strategy in Covalent/Metal-Organic Frameworks Derived Porous Catalysts. *ChemCatChem* **2025**, *17*, e01981, doi:10.1002/cctc.202401981.

[144] Wu, Y.; Wang, L.; Chen, L.; Li, Y.; Shen, K. Morphology-Engineering Construction of Anti-Aggregated Co/N-Doped Hollow Carbon from Metal-Organic Frameworks for Efficient Biomass Upgrading. *Small* **2023**, *19*, 2207689, doi:10.1002/smll.202207689.

[145] Zhao, Q.; Gao, Y.; Zhu, N.; Wang, F.; Zhao, D.; Wang, J. Metal-Organic Frameworks for Energy: From Perfect Crystals to Programmable Defective, Quasi-, and Post-MOFs. *Matter* **2026**, *9*, 102711, doi:10.1016/j.matt.2026.102711.

[146] Lin, S.; Chen, Y.; Li, H.; Wang, W.; Wang, Y.; Wu, M. Application of Metal-Organic Frameworks and Their Derivates for Thermal-Catalytic C1 Molecules Conversion. *iScience* **2024**, *27*, 109656, doi:10.1016/j.isci.2024.109656.

[147] Chen, H.; Shen, K.; Mao, Q.; Chen, J.; Li, Y. Nanoreactor of MOF-Derived Yolk–Shell Co@C–N: Precisely Controllable Structure and Enhanced Catalytic Activity. *ACS Catal.* **2018**, *8*, 1417–1426, doi:10.1021/acscatal.7b03270.

[148] Lü, B.; Qi, W.; Luo, M.; Liu, Q.; Guo, L. Fischer–Tropsch Synthesis: ZIF-8@ZIF-67-Derived Cobalt Nanoparticle-Embedded Nanocage Catalysts. *Ind. Eng. Chem. Res.* **2020**, *59*, 12352–12359, doi:10.1021/acs.iecr.0c00971.

[149] Qin, Y.; Wang, H.; Zhang, H.; Jing, C.; Jia, P.; Zhuo,

L.; et al. Metal–Organic Framework Derived Hierarchical Hollow Materials for High-Performance Zinc–Air Batteries. *J. Mater. Chem. A* **2026**, *14*, 763–782, doi:10.1039/D5TA05575J.

[150] Hu, H.; Liu, J.; Li, W.; Wen, H.; Yang, X.; Ke, B.; et al. MOF-Derived Doped Porous Carbon-Based Catalysts for CO_2 Electroreduction: Design, Mechanisms, and Scale-Up. *Mater. Chem. Front.* **2026**, *10*, 888–921, doi:10.1039/D5QM00888C.